5-1-2012

Structural Performance of Reinforced Concrete Flat Plat Buildings Subjected to Fire

Sara Jean George
University of Nevada, Las Vegas, hippen52@hotmail.com

STRUCTURAL PERFORMANCE OF REINFORCED CONCRETE FLAT PLATE BUILDINGS SUBJECTED TO FIRE

By

Sara Jean George

Bachelor of Science in Architectural Engineering
University of Wyoming
2007

A thesis submitted in partial fulfillment
of the requirements for the

Master of Science Degree in Civil Engineering

Department of Civil and Environmental Engineering
Howard R. Hughes College of Engineering
The Graduate College

University of Nevada, Las Vegas
May 2012

THE GRADUATE COLLEGE

We recommend the thesis prepared under our supervision by

Sara Jean George

entitled

Structural Performance of Reinforced Concrete Flat Plate Buildings Subjected to Fire

be accepted in partial fulfillment of the requirements for the degree of

Master of Science in Civil Engineering
Department of Civil Engineering

Ying Tian, Ph.D., Committee Chair

Samaan Ladkany, Ph.D., Committee Member

Aly Said, Ph.D., Committee Member

Brendan O'Toole, Ph.D., Graduate College Representative

Ronald Smith, Ph. D., Vice President for Research and Graduate Studies
and Dean of the Graduate College

May 2012

ABSTRACT

Structural Performance of Reinforced Concrete Flat-Plate Buildings Subjected to Fire

By

Sara Jean George

Dr. Ying Tian, Examination Committee Chair
Assistant Professor of Civil Engineering
University of Nevada, Las Vegas

Reinforced concrete structures are typically considered to have inherent resistance to fire. However, several concrete structures around the world have experienced partial or total collapse under fire. Reinforced concrete flat-plate is a type of structural system widely used for office and residential buildings. Flat plate construction is prone to punching shear failure at slab-column connections which may lead to a catastrophic progressive collapse. The slabs of flat-plates generally have very thin concrete cover leaving steel reinforcement more sensitive to thermal loads. Little is known in the engineering community about the structural performance of flat-plate structures subjected to fire. Through a detailed nonlinear finite element analysis, this study will examine the internal force and deformation redistribution characteristics of flat-plate structure under fire. Insights gained from this study will create knowledge needed to improve fire-resistant design of flat-plate buildings.

TABLE OF CONTENTS

LIST OF TABLES

LIST OF FIGURES

CHAPTER 1

INTRODUCTION

1.1 General Performance Of Reinforced Concrete Structures In Fire

Following the collapse of the World Trade Center towers in 2001, the structural performance of buildings subjected to fire became a major research focus. Reinforced concrete structures have generally performed well under fire because concrete has a low thermal conductivity and is not combustible. Concrete acts as an insulator and aids in protecting reinforcing bars from significant temperature increase. Accordingly, catastrophic failures of reinforced concrete structures due to fire are uncommon. However, elevated temperatures can alter the thermal and mechanical properties of both concrete and steel reinforcement. The change in these material properties may cause significantly reduced load-carrying capacity and increased deformation of structural members, leading to the risk of large-scale structural failure.

1.2 Historical Events of Concrete Building Collapse due to Fire

Throughout history, the collapses of several concrete buildings have occurred due to uncontrolled fire. A few notable incidents of concrete building collapse due to fire are described in the following.

1.2.1 Delft University of Technology

In May 2008, the Faculty of Architecture Building (Figure 1-1) at Delft University of Technology in the Netherlands experienced partial collapse due to fire. The thirteen story reinforced concrete building caught fire on the 6^{th} floor. The fire was initiated by a coffee vending machine. Rapidly spreading fire restricted firefighters and allowed the fire to burn uncontrolled for seven hours. There were no fatalities, but the building had to be

demolished due to the large extent of the damage (Meacham, Engelhardt, & Kodur, 2009).

Figure 1-1 Collapse of Faculty of Architecture Building (Meacham et al., 2009)

1.2.2 St. Petersburg Apartment Block

A nine-story reinforced concrete apartment building (Figure 1-2) collapsed due to fire in St. Petersburg, Russia in June 2002. It is believed that, during ongoing reconstruction of the site, a gas line was ruptured and fueled the fire (Bietel & Iwankiw, 2008). A large crack appeared in the upper floor leaving residents 20 to 30 minutes to evacuate. The building completely collapsed after burning for one hour. The event killed one person, injured two, and left approximately 430 homeless (*Russian apartment block collapses.*2002).

1.2.3 Egyptian Clothing Factory

A six-story clothing factory (Figure 1-3) in Alexandria, Egypt collapsed after a fire in July 2000. Authorities believed the fire was initiated by an electrical short circuit within the reinforced concrete building. The fire spread rapidly and took firefighters seven hours

to extinguish. When the fire appeared to be put out, the building suddenly collapsed, killing at least 15 people and injuring many others. The estimated cost of the destruction was $2.5 million (*Factory fire kills 15 in egypt.*2000).

Figure 1-2 Collapse of St. Petersburg Apartment Block (*Russian apartment block collapses.*2002)

Figure 1-3 Collapse of clothing factory in Alexandria, Egypt (*Factory fire kills 15 in egypt.*2000)

1.2.4 Katrantzos Sports Department Store

The Katrantzos Sports Department Store (Figure 1-4) in Athens, Greece partially collapsed during a fire in December 1980. The fire started on the 7th floor of the eight-

story reinforced concrete building. Rapid spread of the fire was facilitated by an unprotected escalator and lift shaft. Aluminum panels utilized on the facade melted, allowing sufficient ventilation for the fire to fully develop. The exact cause of the fire was never confirmed, but evidence pointed to arson (Papaioannou, 1986).

Figure 1-4 Collapse of Katrantzos Sports Department Store (Papaioannou, 1986)

1.3 Introduction to Reinforced Concrete Flat Plate Structures

Reinforced concrete floor slabs are one of the most common structural elements. Flat slab is a beamless system with support at the columns. There are three types of flat slabs used for reinforced concrete buildings: flat slab with drop panels (Figure 1-5a), flat slab with both drop panels and column capitals (Figure 1-5b), and flat slab of uniform thickness (Figure 1-5c), more commonly referred to as flat plate. Flat plate construction is normally used in structures where low gravity loads are found such as residential buildings and some office buildings. When used in regions with high seismicity, flat plate

is designed as a gravity load-carrying system and lateral loads are resisted by conjunctionally used shear walls or perimeter moment frames (Park & Gamble, 2000).

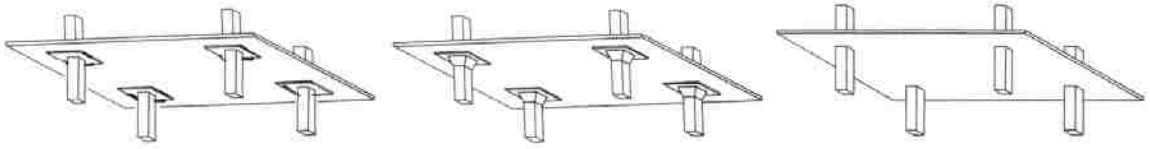

(a) Flat slab with drop panels (b) Flat slab with drop panels and column capitals (c) Flat plate

Figure 1-5 Classification of flat slab construction (Park & Gamble, 2000)

The slab thickness of a flat plate structure is generally controlled by the design code provisions regarding the two-way shear resistance or deflection serviceability. Consequently, the ratio of slab top reinforcement resisting negative bending moment at the slab-column connections is normally less than 1.0% (Sherif & Dilger, 1996). The reinforcement ratio for slab bottom bars resisting positive moment is even lower because their design is often governed by the minimum slab reinforcement requirements.

Flat plates are most commonly controlled by punching shear at columns. Punching shear can be a brittle failure that occurs due to the highly concentrated bending moment and shear in the slab at the vicinity of the column. The concern for punching failure is, even though it happens locally, the gravity load carried initially by the failed slab-column connection will be transferred to the surrounding connections. If these connections cannot handle the redistributed loads, a chain reaction of punching failure over the entire floor will be triggered, resulting in a large-scale or even complete collapse of the building. To avoid punching failure, shear reinforcement such as shear studs can be installed in a flat plate structure under the following situations: (1) slab-column connections need to

transfer large unbalanced moment caused by pattern or lateral loads; (2) heavy gravity loads act on the slab; or (3) relatively large span length is used in the system.

1.4 MOTIVATION OF RESEARCH

The research presented in this thesis is motivated by the existing gap in knowledge regarding the vulnerability of punching failure and the associated risk of progressive collapse in flat plate structures subjected to fire-induced elevated temperatures. Extremely limited information is available to date for this subject.

Compared with beams or columns, slabs have a lower design code requirement for minimum concrete cover and thus less protection for reinforcement from fire-induced elevated temperature. It is known that a moment frame structure can survive from fire without large-scale collapse if the beams as well as the slabs can develop catenary action. However, flat plates may not be able to achieve an effective catenary action because only a few slab bottom reinforcing bars are anchored into the columns, and the bars may lose their tensile strength at high temperature. Additionally, the slab top reinforcement at columns will strip out of the slab if a punching failure occurs, making it difficult to carry vertical loads. Once a punching failure occurs, the slab-column connection may completely lose its gravity loading capacity. It is critical for flat plates to avoid any punching failure under fire loading.

It is expected that a flat plate under a long-duration fire experiences significant load redistribution. At ambient temperature, uniformly distributed gravity loads (Figure 1-6a) cause positive bending moment at slab mid-span and negative moment near the columns (Figure 1-6b). When a fire load is applied beneath the slab, columns restrain slab flexural deformation induced by thermal gradient, resulting in increased slab negative bending

moment near the columns. Moreover, the top reinforcement remains relatively cool while bottom reinforcement heats up. The elevated temperature may cause the bottom bars at mid-span to yield at low stress. A yielded region with significantly reduced flexural capacity forms in the slab (Figure 1-6c), causing the bending moment to be further redistributed (Figure 1-6d) to the surrounding columns. The load redistribution due to restrained flexural deformation and bottom reinforcement yielding in the slab, lead to much higher negative moment and large inelastic flexural deformation demand at these locations, which will likely result in a punching failure of the flat plate structure.

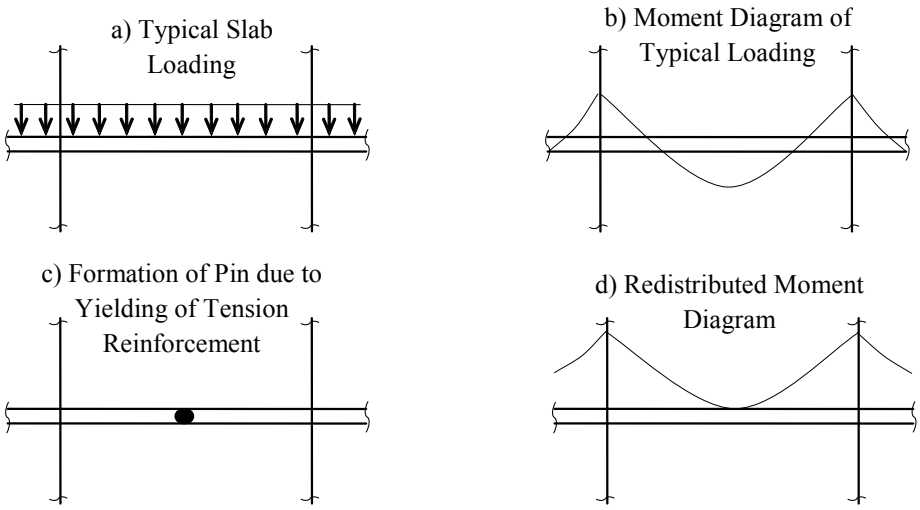

Figure 1-6 Moment Redistribution under Fire

1.5 Research Objectives, Scope, and Methodology

The overall objective of this study is to examine the punching failure potential of slab-column connections in flat plate buildings experiencing fire. The research is limited to flat plates where the design of slabs is governed by gravity loads and the slabs are supported on square columns without using any shear reinforcement.

To achieve the aforementioned goal, nonlinear finite element analyses are performed on a prototype flat plate structure subjected to fire as well as service level gravity loads. To minimize the uncertainties involved in the analyses, the modeling parameters for mechanical and thermal properties of materials are calibrated from relevant test data. The analyses determine the slab local force and deformation demands at columns, which are then compare with the strength and deformation capacity of slab-column connections at elevated temperatures to identify the likelihood of punching failure of slabs subjected to fire loading.

1.6 Outline of Thesis

Chapter 2 reviews previous studies for the gravity capacity of flat plate structures, thermal and mechanical properties of concrete and steel under elevated temperature, and an analytical study of the structural performance of a flat plate building under fire. The study (presented in Chapter 3 and 4) is performed by fulfilling the following tasks:

Task 1 (Chapter 3): Calibrate the mechanical modeling parameters of materials for finite element analysis based on the test data of slab-column connections under gravity loading in ambient temperature.

Task 2 (Chapter 3): Calibrate the modeling parameters for material properties under elevated temperature based on test data of two-way slabs under fire loading.

Task 3 (Chapter 4): Design a multi-story prototype flat plate building in accordance with the current building design codes.

Task 4 (Chapter 4): Using the modeling parameters calibrated from Tasks 1 and 2, conduct finite element analyses of the prototype building subjected to both gravity and fire loads. The punching shear strength estimated based on the localized slab rotation is

compared with the gravity shear acting on the slab-column connections to determine the risk of punching failure in a flat plate structure.

Finally, Chapter 5 summarizes the findings from this research and suggestions for further studies.

CHAPTER 2

LITERATURE REVIEW

2.1 BEHAVIOR OF SLAB-COLUMN CONNECTIONS UNDER GRAVITY LOADING

Numerous tests have been conducted to study the shearing capacity of flat plates. Test specimens were generally isolated slab-column connections, each containing a square slab and a centrally located column stub. The slab edges simulated the approximate location of inflection points of slabs subjected to concentric gravity loading. Vertical loads, introducing both bending moment and shear, were applied to the specimens at either the center column or slab edges. Three studies most relevant to the present research are described as follows.

2.1.1 Experimental Study by Elstner and Hognestad (1956)

Elstner and Hognestad (1956) conducted a series of tests involving 39 specimens. The effects of concrete strength, slab tensile reinforcement ratio, column size, loading approach (concentric *vs.* eccentric), and supporting conditions were examined. Figure 2-1 shows the load-center deflection response of a group of specimens subjected to concentric gravity loading. The load-deformation responses are aligned in this figure according to slab tensile reinforcement ratio. Specimen B-14 had the highest reinforcement ratio (3.0%) and Specimens B-2 and B-1 had the lowest reinforcement ratio (0.5%). This figure clearly indicates that slab tensile reinforcement ratio is a parameter governing the behavior of a slab-column connection. Specimens with a reinforcement ratio less than 1.0% developed general yielding as indicated by the rapidly increased deflection following the peak load. Additionally, yielding of slab tensile

reinforcement near the column (indicated by P_{yield} in the figure) occurred in almost all the specimens (even with high reinforcement ratios) prior to their ultimate punching failure.

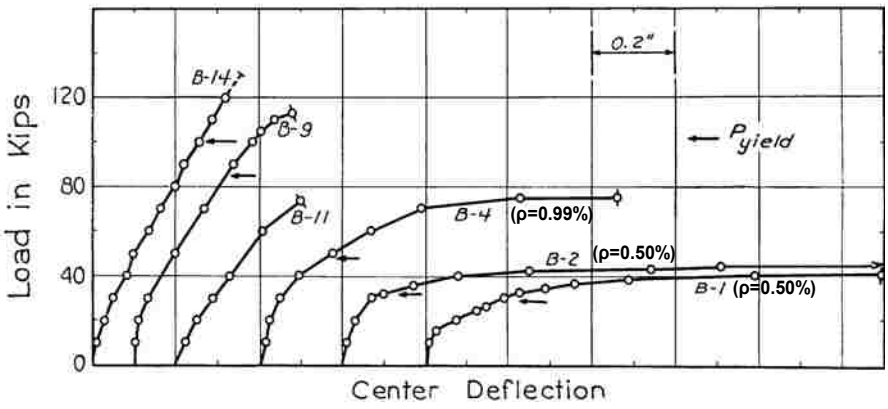

Figure 2-1 Load-center deflection response of slab-column connections under concentric gravity loading (Elstner & Hognestad, 1956)

It is noteworthy, from Figure 2-1, that for connections with low-to-moderate reinforcement ratios typical in actual applications, punching failure was caused by excessive deformation rather than reaching a critical value of shear. Because the loading capacity of these specimens was larger than that evaluated from yield line theory, their failure was defined as flexural failure. Even though these specimens eventually failed in punching due to inclined cracking, the punching failure was treated as secondary. In more recent studies, punching failure of flat plates, regardless of the reinforcement ratio, were exclusively classified as shear failure.

2.1.2 Experimental Study by Guandalini, Burdet and Muttoni (2009)

Guandalini, Burdet, and Muttoni (2009) tested eleven isolated slab-column specimens with slab tensile reinforcement ratios less than 1.5% and without shear reinforcement. A concentrated vertical load, simulating gravity load effects, was applied through the center column. Even though the main focus of the study was to investigate the size effects (scale

of test specimen) on the punching capacity of lightly reinforced slab-column connections, the tests revealed important information regarding the deformation characteristics of the slab prior to its final punching failure. Figure 2-2 shows the measured deflections of both top and bottom slab surfaces at nine locations as a function of the applied load level. This figure clearly demonstrates that, for a lightly reinforced flat plate, the slab deflection can be attributed primarily to rigid body rotation. This rotation, similar to that of plastic hinges in beams or columns, is due to the highly localized slab deformation near the column caused by concrete cracking and flexural reinforcement yielding.

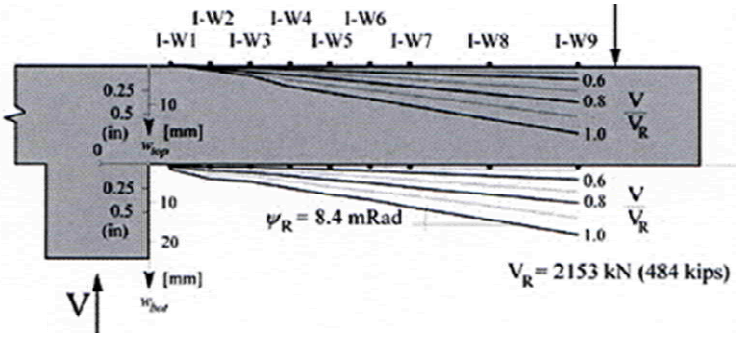

Figure 2-2 Deflection of slab-column connection (Guandalini, Burdet, & Muttoni, 2009)

2.1.3 Analytical Study by Moss, Dhakal, Wang, and Buchanan (2008)

Moss, Dhakal, Wang, and Buchanan (2008) conducted numerical simulations of a flat plate building subjected to fire. The building was 3-bay by 3-bay in plan with columns 6 meters apart. The slab was 0.2 m thick. Moment frames were deployed along the building perimeter. SAFIR, a finite element program, was used as the analysis platform. The slabs and columns were simulated using shell elements and line elements, respectively. Due to symmetry of the building, only a quarter of the structure was modeled in the analyses, as shown in Figure 2-3. Two ISO 834 four hour duration fires, one with and another one without decay phase, were considered and applied below the slab of the lowest story.

Gravity loads including the dead load and 40% of the live load were applied to the slab. The analyses focused primarily on the vertical deflection, horizontal expansion, bending moment, and in-plane force characteristics of the slab.

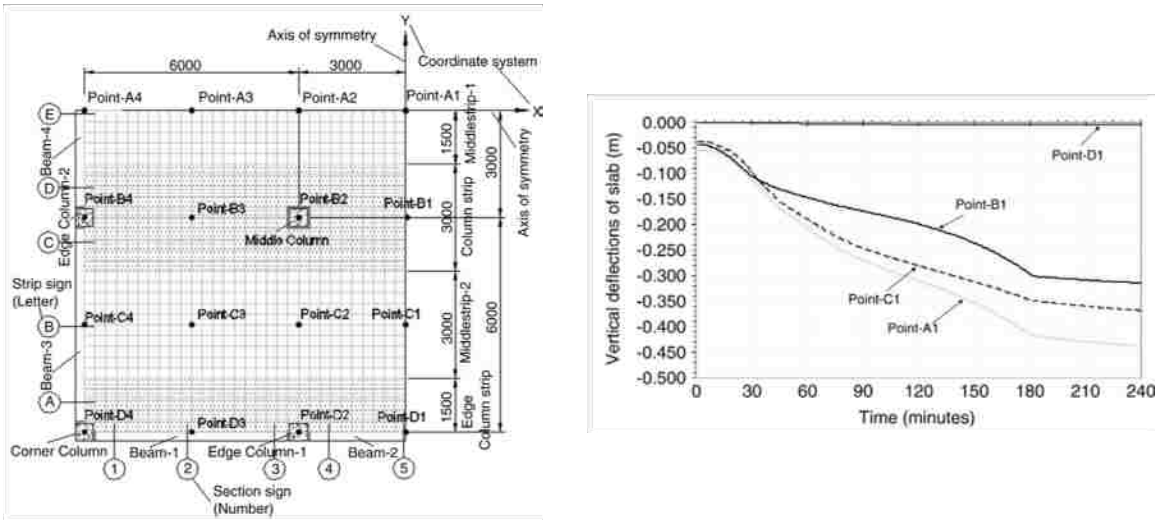

Figure 2-3 Analysis model and slab vertical deflections (Moss, Dhakal, Wang, & Buchanan, 2008)

Under the four hour fire, the slab deformed as a 3-D catenary, creating a large curvature around the column perimeter so that the slab seemed to be hanging on the columns. Figure 2-3 also shows the slab vertical deflection at various mid-span locations for a quarter of the structure. The center of the entire floor (Point A1) experiences the greatest deflection while Point D1, located at the mid-span of the perimeter beam, experiences virtually negligible deflection.

Because the fire loads were applied to the entire story, the elevated temperature caused little change in the vertical shear transferred between slab and column. Although it was pointed out that the large curvature of slab under elevated temperature may cause punching failure, no study was further conducted to identify how the shear strength of the slab will deteriorate with increase in temperature and the likelihood of punching failure.

2.2 STANDARD FIRE TESTING

Standard fire test experimentally or numerically assesses the material and structural performance of a specimen. During a test, a structural component or system is loaded to produce a state of stress comparable to that in an actual condition under gravity loading. A prescribed thermal load, defined as temperature history, is then applied to the test specimen (Purkiss, 1996). For concrete slabs, fire load is applied below the slab. There are two reasons for this approach. First, fire tends to spread upwards rather than downwards. Second, the most vulnerable part of the slab is usually the underside since there is no debris to provide protection form fire. Fire-resistance testing is included in many standards such as the British Standard BS 476 Parts 20-23, Canadian Standard CAN/ULC-S101-M89, Australian Standard AS 1530 Part 4, American Standard ASTM E119, and International Standard ISO 834. Most standards are based on the widely adopted ASTM E119 or ISO 834 (Buchanan, 2001).

2.3 TIME-TEMPERATURE CURVE

To perform physical testing or numerical simulation of structural components under fire, an estimated time history of temperature encountered in an actual fire is needed. ASTM E119 and ISO 834 provide similar time-temperature curves as shown in Figure 2-4. The ISO 834 specifies temperature T (℃) as

$$T = 345\log_{10}(8t + 1) + T_0 \qquad \text{Equation 2-1}$$

where t is time (minutes) and T_0 is ambient temperature (˚C). ASTM E119 defines the temperature history using a series of discrete points. Lie (1992) developed Equation 2-2 to represent the ASTM E119 time-temperature curve as

$$T = 750\left[1 - \mathrm{e}^{-3.79553\sqrt{t_h}}\right] + 170.41\sqrt{t_h} + T_0 \qquad \text{Equation 2-2}$$

where t_h is time (hours).

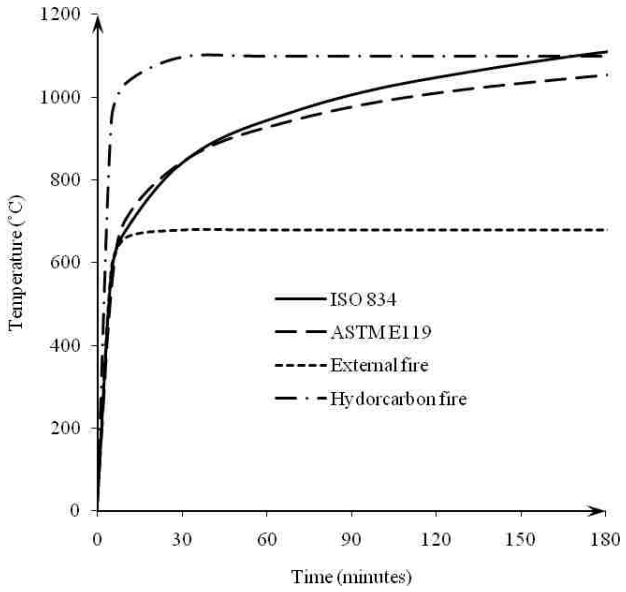

Figure 2-4 Standard time-temperature curves (Buchanan, 2001)

Eurocode 1 (EC1, 1996) considers two alternative design fires shown in Figure 2-4: hydrocarbon fire and external fire. The hydrocarbon fire curve, defined in Equation 2-3, is used for structural members subjected to a large pool fire and engulfed in flames. The external fire, given in Equation 2-4, is used for members located outside a burning compartment and thus experiencing lower temperatures.

$$T = 1080(1 - 0.325e^{-0.167t} - 0.313e^{-3.8}) + T_0 \quad \text{Equation 2-3}$$

$$T = 660(1 - 0.687e^{-0.32t} - 0.313e^{-3.8t}) + T_0 \quad \text{Equation 2-4}$$

2.4 Thermal Properties of Concrete

2.4.1 Thermal Conductivity (λ_c)

Thermal conductivity, λ_c, is a measure of the rate of heat transferred through a unit thickness of material, or the ratio of heat flux to temperature gradient. The thermal conductivity of concrete varies greatly with temperature (Buchanan, 2001). Two sources, the study by Lie (1992) and Eurocode 2 (EC2, 1995), can be used to assess the thermal

conductivity of concrete. Each correlates λ_c with concrete aggregate type (siliceous concrete *vs*. calcareous concrete). Lie (1992) defined λ_c (W/m˚C) as:

Siliceous Concrete

$$\lambda_c = \begin{cases} -0.000625T + 1.5 & 0 \le T \le 800^{\circ}\text{C} \\ 1.0 & T > 800^{\circ}\text{C} \end{cases} \qquad \text{Equation 2-5}$$

Calcareous Concrete

$$\lambda_c = \begin{cases} 1.355 & 0 \le T \le 293^{\circ}\text{C} \\ -0.001241T + 1.762 & T > 800^{\circ}\text{C} \end{cases} \qquad \text{Equation 2-6}$$

EC2 (1995) defines λ_c (W/mK) as:

Siliceous Concrete

$$\lambda_c = 2 - \frac{0.24T}{120} + 0.012\left(\frac{T}{120}\right)^2 \qquad 20 \le T \le 1200^{\circ}\text{C} \qquad \text{Equation 2-7}$$

Calcareous Concrete

$$\lambda_c = 1.6 - \frac{0.16T}{120} + 0.008\left(\frac{T}{120}\right)^2 \qquad 20 \le T \le 1200^{\circ}\text{C} \qquad \text{Equation 2-8}$$

Figure 2-5 graphically compares the concrete thermal conductivity defined by Equations 2-5 through 2-8. It is seen that λ_c has similar values for the two types of concrete if temperature is between 300˚C and 800˚C. For simplicity it is permissible to use 1.6W/mK for siliceous concrete and 1.3W/mK for calcareous concrete (European Committee for Standardization, 1995a).

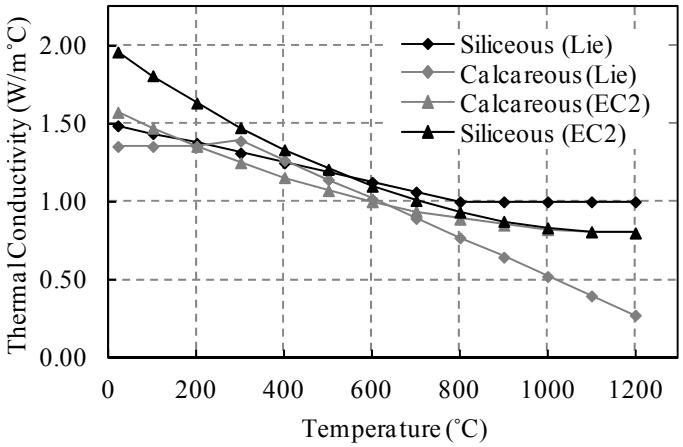

Figure 2-5 Thermal conductivity of concrete

2.4.2 Specific Heat (c_c)

Specific heat, c_c, is the amount of heat required to raise temperature by one degree per unit mass. The specific heat of concrete varies with both moisture content and aggregate type. Moisture is driven off during the heating process. The effects of moisture content on concrete specific heat become insignificant when temperatures are greater than 200˚C. A peak value of c_c is given in EC2 (1995) for concrete with high moisture content. The peak value occurs between 100 and 200˚C and can be taken as 1875 J/kgK for concrete with 2% humidity and 2750 J/kgK for concrete with 4% humidity (European Committee for Standardization, 1995a). Equation 2-9 suggested by Lie (1992) describes c_c for siliceous concrete. Equation 2-10 from EC2 (1995) gives the definition of c_c (J/kgK) for both siliceous and calcareous concrete.

$$\rho_c c_c = \begin{cases} (0.005T + 1.7) \times 10^6 & 0 \le T \le 200^\circ\text{C} \\ 2.7 \times 10^6 & 200 \le T \le 400^\circ\text{C} \\ (0.013T - 2.5) \times 10^6 & 400 \le T \le 500^\circ\text{C} \\ (-0.013T + 10.5) \times 10^6 & 500 \le T \le 600^\circ\text{C} \\ 2.7 \times 10^6 & T > 600^\circ C \end{cases} \quad \text{J/m}^3{}^\circ\text{C} \qquad \text{Equation 2-9}$$

where ρ_c is the density of concrete.

$$c_c = 900 + \frac{80T}{120} - 4\left(\frac{T}{120}\right)^2 \qquad 20 \le T \le 1200℃$$ Equation 2-10

Figure 2-6 shows the specific heat of concrete formulated by EC2 (1995) and Lie (1992) at various temperatures. The two sources predict similar specific heat properties for siliceous aggregate concrete; however, the curve based on Lie's suggestion spikes between 400 and 600˚C due to the assumed presence of quartz, whose composition alters at this temperature range. For simplicity, EC2 (1995) allows taking specific heat as 1000 J/kgK for both siliceous and calcareous aggregate concrete.

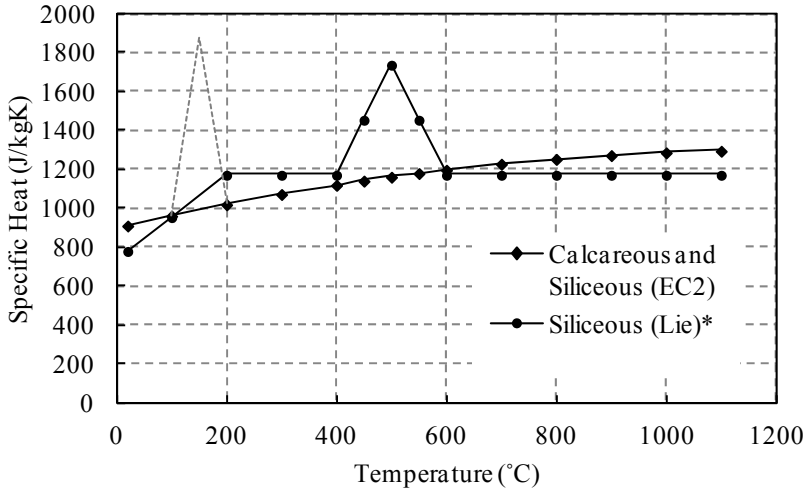

Figure 2-6 Specific heat of concrete (* ρ_c was taken as 2300 kg/m^3)

2.4.3 Thermal Expansion

Thermal expansion defines the strain of unrestrained material due to heat. For concrete, thermal expansion is mainly affected by aggregate type and generally nonlinear with respect to temperature. The nonlinearity is due in part to the chemical or physical changes in aggregate and the thermal incompatibilities between aggregate and matrix. Moisture within concrete may also affect thermal expansion by causing shrinkage when water is being driven from the material (Purkiss, 1996). Several formulations of thermal

expansion (strain), ε_{th}, have been provided. EC2 (1995) defines concrete thermal expansion as:

Siliceous Concrete

$$\varepsilon_{th} = \begin{cases} -1.8 \times 10^{-4} + 9 \times 10^{-6}T + 2.3 \times 10^{-11}T^3 & 20 \leq T \leq 700^{\circ}\text{C} \\ 14 \times 10^{-3} & 700 < T \leq 1200^{\circ}\text{C} \end{cases} \quad \text{Equation 2-11}$$

Calcareous Concrete

$$\varepsilon_{th} = \begin{cases} -1.2 \times 10^{-4} + 6 \times 10^{-6}T + 1.4 \times 10^{-11}T^3 & 20 \leq T \leq 805^{\circ}\text{C} \\ 12 \times 10^{-3} & 805 < T \leq 1200^{\circ}\text{C} \end{cases} \quad \text{Equation 2-12}$$

EC2 (1995) also allows a simplification of $\varepsilon_{th} = 18 \text{ x } 10^{-6}T$ for siliceous concrete and $\varepsilon_{th} = 12 \text{ x } 10^{-6}T$ for calcareous concrete. It is difficult to separate thermal strain and shrinkage from test results. These simplified definitions for concrete thermal strain have included the effects of shrinkage caused by the removal of moisture (Buchanan, 2001).

Another recommendation for determining concrete thermal expansion was made by Lie (1992). In this model an equation is given for the coefficient of thermal expansion (α) for both siliceous and calcareous concrete as:

$$\alpha = (0.008\text{T} + 6) \times 10^{-6} \quad \text{Equation 2-13}$$

Figure 2-7 illustrates this formulation together with the definition of concrete thermal expansion by EC2 (1995). Little difference exists between the EC2 model for calcareous concrete and Lie's model until approximately 600˚C, after which discrepancy becomes noticeable. In comparison between Lie's model and EC2 model for siliceous concrete, there is much disagreement.

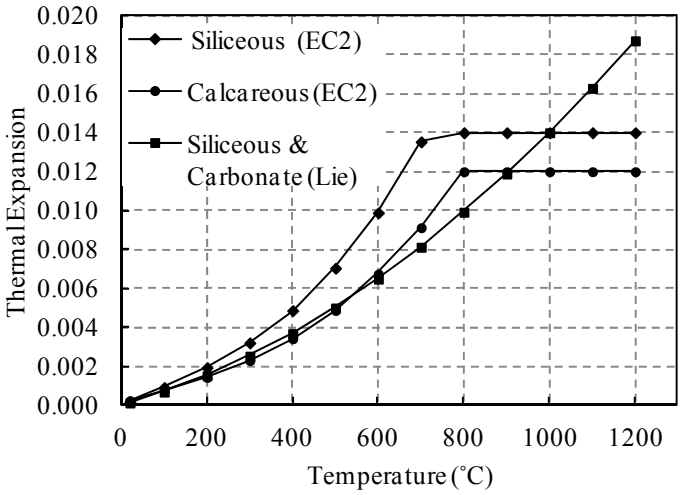

Figure 2-7 Thermal expansion of concrete

2.4.4 Spalling

Concrete cover may spall off a member when it is subjected to fire (Figure 2-8). Spalling exposes the steel reinforcement to heat and may reduce the load-carrying capacity of the member due to the decreased strength of steel at high temperature. Spalling is not well understood because it is a function of many factors including the type of aggregate, thermal stresses near corners, and type of cement paste.


Figure 2-8 Spalling at corner of concrete beam subjected to fire (Buchanan, 2001)

Spalling is often related to water evaporation from cement paste during heating. High pore pressures can create tensile stresses that exceed the tensile strength of concrete. Experiments revealed high susceptibility to spalling for concrete members with high moisture content, rapid heating, high slenderness, and high level of stress (Buchanan, 2001). Note that the explosive spalling of concrete is still poorly understood because it is one of the most complex properties of concrete under high temperature (Fletcher, Welch, Torero, & Usmani, 2007). Consequently, there is a lack of definitive design guidance among the various building design codes.

2.5 Thermal Properties of Steel

2.5.1 Thermal Conductivity (λ_s)

The thermal conductivity of steel was found to depend slightly on its strength, but due to its insignificance, such an effect can be neglected (Purkiss, 1996). Eurocode 3 (EC3, 1995) gives λ_s (W/mK) of steel as a function of temperature per Equation 2-14, which is shown in Figure 2-9. For simplicity, λ_s can be approximated as 45W/mK.

$$\lambda_s = \begin{cases} 54 - 0.0333T & 20 \le T \le 800^\circ\text{C} \\ 27.3 & 800 < T \le 1200^\circ\text{C} \end{cases} \qquad \text{Equation 2-14}$$

2.5.2 Specific Heat (c_s)

The specific heat for steel varies with temperature as shown in Figure 2-10. A sharp change in specific heat occurs around 730-750˚C. It is generally acceptable to use 600 J/kgK for simple calculations, but a more accurate result for c_s (J/kgK) can be obtained from Equation 2-14 (European Committee for Standardization, 1995b).

$$c_s = \begin{cases} 425 + 0.773T - 0.00169T^2 + 2.22 \times 10^{-6}T^3 & 20 \le T \le 600^\circ\text{C} \\ 666 + 13002/(738 - T) & 600 < T \le 735^\circ\text{C} \\ 545 + 17820/(T - 731) & 735 < T \le 900^\circ\text{C} \\ 650 & 900 < T \le 1200^\circ\text{C} \end{cases} \qquad \text{Equation 2-15}$$

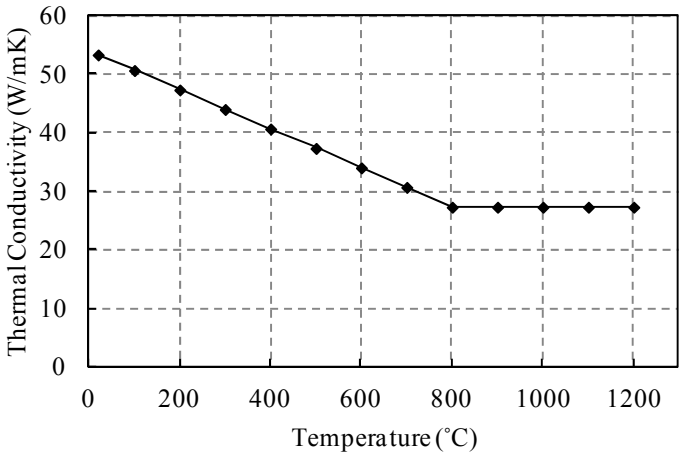

Figure 2-9 Thermal conductivity of steel

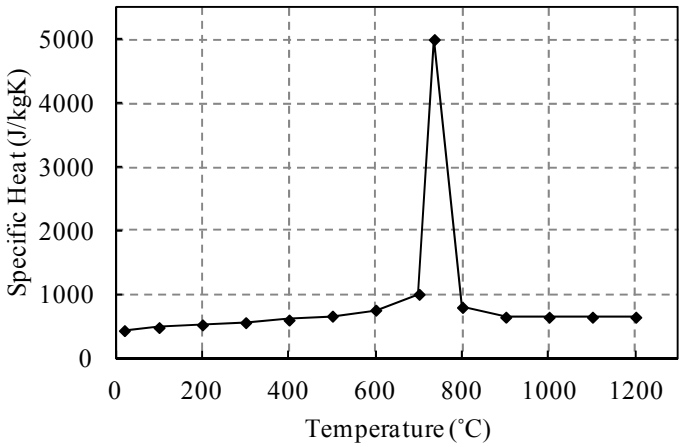

Figure 2-10 Steel specific heat

2.5.3 Thermal Expansion

The coefficient of thermal expansion of steel can usually be taken as $11.7 \times 10^{-6}/^{\circ}\mathrm{C}$ at room temperature and increases at higher temperatures with a plateau between 700 and 800˚C (Buchanan, 2001). The thermal expansion of structural and reinforcing steel according to EC3 (1995) is given in Equation 2-16 and Figure 2-11. A linear approximation of $\varepsilon_{th} = 14 \times 10^{-6}(T - 20)$ may also be taken for simplicity.

$$\varepsilon_{th} = \begin{cases} 1.2 \times 10^{-5}T + 0.4 \times 10^{-8}T^2 - 2.416 \times 10^{-4} & 20 \le T \le 750^{\circ}\mathrm{C} \\ 1.1 \times 10^{-2} & 750 < T \le 860^{\circ}\mathrm{C} \\ 2 \times 10^{-5}T - 6.2 \times 10^{-3} & 860 < T \le 1200^{\circ}\mathrm{C} \end{cases} \quad \text{Equation 2-16}$$

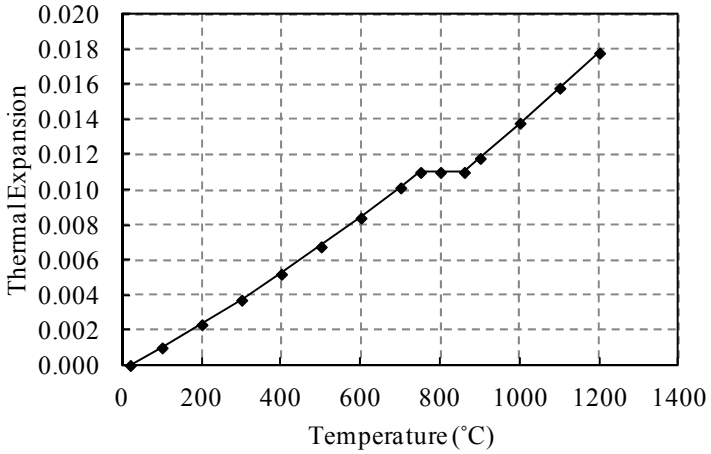

Figure 2-11 Thermal expansion of steel

2.6 Mechanical Properties of Concrete at Elevated Temperatures

2.6.1 Total Strain (ε)

The total strain of concrete consists of four components: thermal strain (ε_{th}), stress related strain (ε_{σ}), creep strain ($\varepsilon_{c\sigma}$), and transient strain (ε_{tr}). Thermal strain (also known as thermal expansion), which has been discussed in Section 2.5.3, is a function of temperature only. Stress-related, creep, and transient strains depend on both stress and temperature. In addition, creep strain is also a function of time (Buchanan, 2001).

Stress-related strain encompasses the elastic and plastic components of strain. Typical stress-strain relationships can be seen in Figure 2-12 for normal strength concrete. As temperature increases the concrete compressive strength drops while the strain at peak stress increases. Table 2-1 provides the recommended characteristic values of stress and strain at different temperatures.

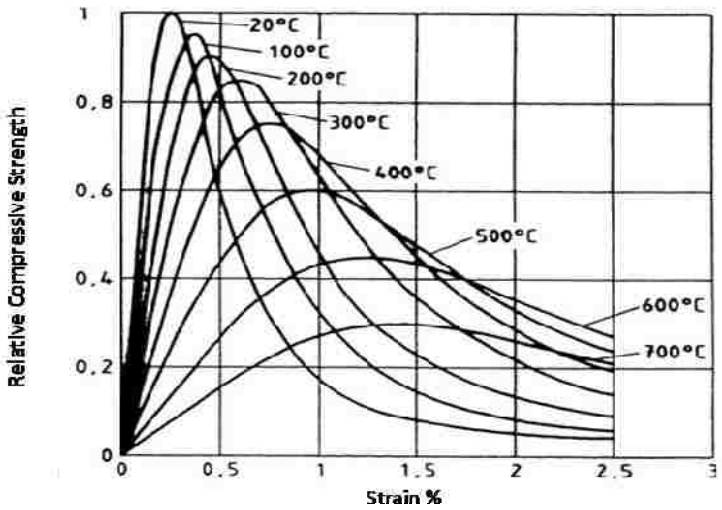

Figure 2-12 Concrete stress-strain responses at elevated temperatures (European Committee for Standardization, 1995a)

Table 2-1 Characteristic stress-strain curve values for concrete (European Committee for Standardization, 1995a)

Temperature (˚C)	Concrete Stress (% of f_c)		Strain at peak stress	Ultimate Strain
	Siliceous	Calcareous	$\varepsilon_{c1}(10^{-3})$	$\varepsilon_{cu}(10^{-3})$
20	1	1	2.5	20
100	0.95	0.97	3.5	22.5
200	0.9	0.94	4.5	25
300	0.85	0.91	6	27.5
400	0.75	0.85	7.5	30
500	0.6	0.74	9.5	32.5
600	0.45	0.6	12.5	35
700	0.3	0.43	14	37.5
800	0.15	0.27	14.5	40
900	0.08	0.15	15	42.5
1000	0.04	0.06	15	45
1100	0.01	0.02	15	47.5

Creep, a type of long-term deformation of materials, is prominent for members under high permanent loads. When a concrete structural component is subjected to fire, creep strain becomes much more problematic because it can accelerate as the load-carrying capacity reduces. Figure 2-13 shows the creep strain data for a concrete specimen stressed at $0.225f_c$ and $0.45f_c$ at elevated temperature respectively.

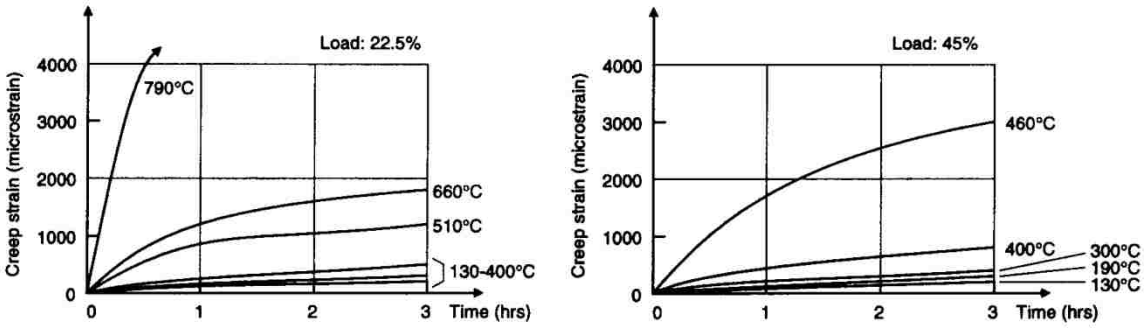

Figure 2-13 Concrete isothermal creep at elevated temperatures (Anderberg & Thelandersson, 1976)

Transient strain is unique to concrete and closely related to creep strain. Transient strain is largely due to the thermally induced incompatibilities between aggregate and cement. Transient strain is experienced only during the first cycle of heating and cooling. Studies have been conducted to predict transient strain, but true measurements can only be obtained by removing thermal strain, creep strain and stress-related strain from the measured total strain (Purkiss, 1996).

2.6.2 Modulus of Elasticity (E_c)

Figure 2-14a shows concrete modulus of elasticity, E_c, as a function of temperature for three types of concrete. E_c decreases linearly with temperature for carbonate concrete but nonlinearly for siliceous and lightweight concrete. Siliceous concrete experiences quick decrease in E_c at approximately 900˚C. EC2 (1995) recommends Equations 2-17 and 2-18, represented in Figure 2-14b, for estimating E_c of siliceous concrete at elevated temperatures. These equations are considered conservative for concrete with other types of aggregate.

$$E_c(T) = \left(k_c(T)\right)^2 \times E_c(20^{\circ}\mathrm{C}) \qquad \text{Equation 2-17}$$

where

$$k_c(T) = \begin{cases} 1 & 20 \le T \le 100^{\circ}\mathrm{C} \\ (1600 - T)/1500 & 100 < T \le 400^{\circ}\mathrm{C} \\ (900 - T)/625 & 400 < T \le 900^{\circ}\mathrm{C} \\ 0 & T > 900^{\circ}C \end{cases}$$ Equation 2-18

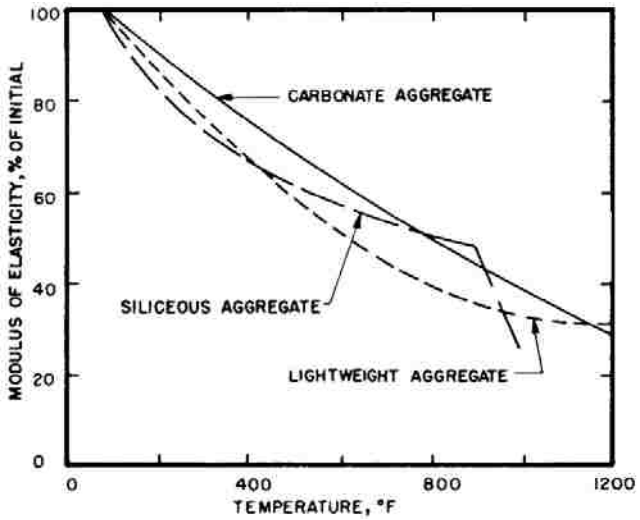

(a) (CRSI Committee of Fire Ratings, 1980)

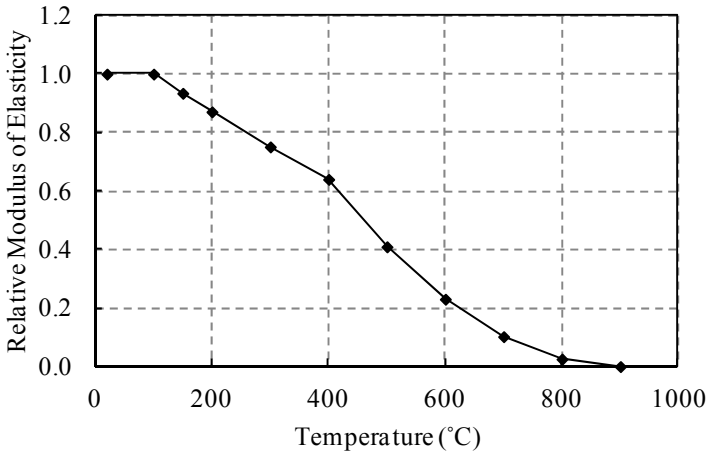

(b) (European Committee for Standardization, 1995a)

Figure 2-14 Concrete modulus of elasticity of at elevated temperatures

2.6.3 Compressive Strength (f_c)

Concrete compressive strength, f_c, at high temperature is also affected by aggregate type. Siliceous concrete tends to lose strength at a faster rate than calcareous or lightweight concrete (Schneider, 1988). Figure 2-15a summarizes the results of previous studies. Concrete strength remains relatively high until 400˚C, after which it decreases

rapidly. Equation 2-19 with the use of coefficient $k_c(T)$ in Equation 2-18 defines f_c as a function of temperature. Figure 2-15b graphically illustrates the relationship between the relative compressive strength $k_c(T)$ and temperature. Table 2-1 from EC2 (1995) also provides design recommendations for f_c reduction due to temperature increase.

$$f_c(T) = k_c(T) \times f_c(20^{\circ}\text{C}) \qquad \text{Equation 2-19}$$

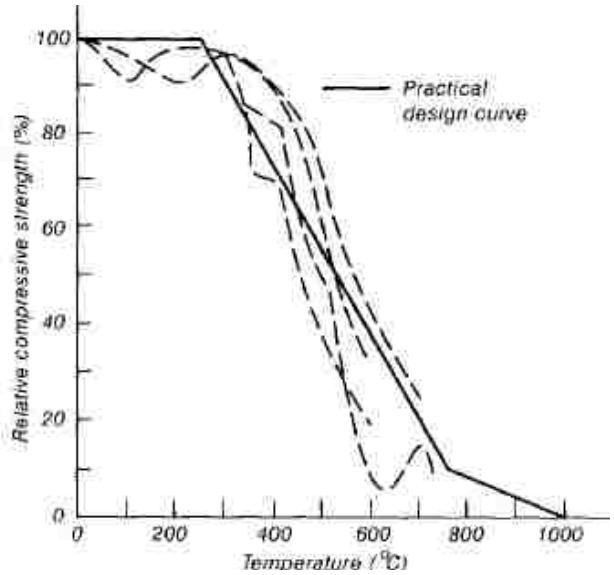

(a) (Schneider, 1988)

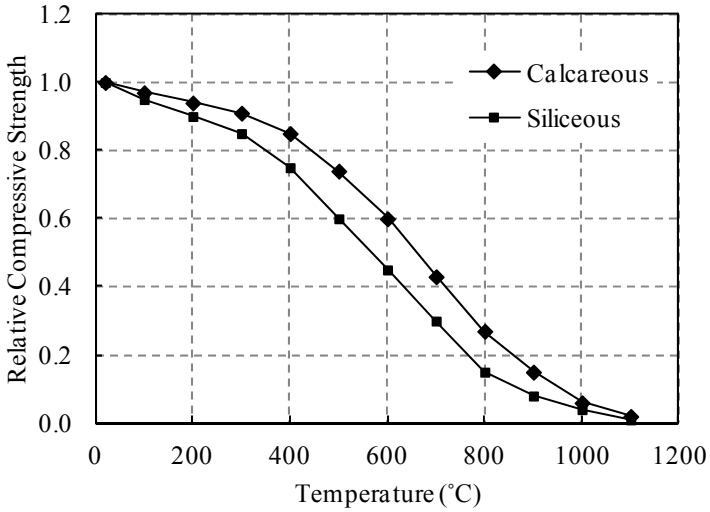

(b) Siliceous concrete (European Committee for Standardization, 1995a)

Figure 2-15 Effect of temperature on concrete compressive strength

2.6.4 Tensile Strength (f_t)

The tensile strength of concrete, f_t, is very low when compared to its compressive strength. For this reason f_t is often assumed negligible, which is conservative for design purposes. ACI 318-08 (2008) defines the modulus of rupture, f_r, (psi), or flexural tensile strength as a function of compressive strength per Equation 2-20.

$$f_r = 7.5\sqrt{f_c} \qquad \text{Equation 2-20}$$

The modulus of rupture is a measure of tensile strength taken by subjecting a plain concrete beam or slab to bending (Nilson, Darwin, & Dolan, 2003). When it is necessary to account for f_t under elevated temperature, EC2 (1995) suggests using Figure 2-16, where $k_{ct}(\theta)$ is the relative tensile strength. As temperature increases, f_t decreases linearly until 600˚C where it is assumed to be zero.

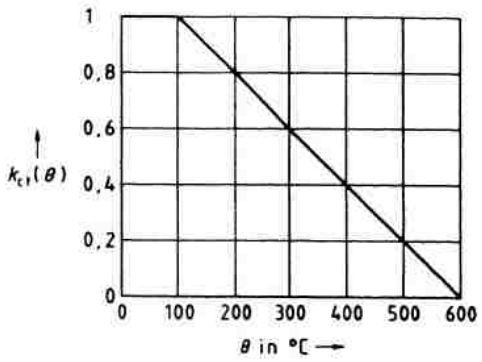

Figure 2-16 Effect of temperature on concrete tensile strength

2.7 Mechanical Properties of Steel at Elevated Temperature

2.7.5 Total Strain

The total strain of steel under elevated temperature contains three components: thermal strain, stress-related strain, and creep strain. Different from concrete, transient

strain does not exist in steel. Thermal strain (ε_{th}) is the thermal expansion of steel at elevated temperatures and has been discussed in Section 2.5.3.

Steel at elevated temperatures experiences substantial strength as well as stiffness degradation. The relationship of stress-related strain for steel can be obtained by direct steady-state testing at elevated temperatures or by transient tests (Buchanan, 2001). Figure 2-17 provides a set of typical stress-strain curves for hot-rolled and cold-worked reinforcing steel. Normal strength steel has well-defined yield strength at or slightly above ambient temperatures. However, no true yield point exists under high temperatures.

Creep strain is relatively insignificant for steel at normal temperatures. As temperature reaches 400 to 500˚C creep becomes pronounced. Figure 2-18 shows typical creep test data of steel in tension. It can be seen that creep depends highly on both temperature and stress level. The creep strain increases sharply once a temperature threshold is reached. Moreover, creep strain of steel can be sensitive to its composition (Purkiss, 1996).

2.7.6 Modulus of Elasticity (E_s)

The steel modulus of elasticity, E_s, decreases as temperature increases. The reduction rate varies according to the type of steel such as structural, pre-stressed, or reinforcing steel. Figure 2-19 shows the reduction rate of E_s for each steel type. The modulus of elasticity for reinforcing steel deteriorates the quickest among the three types of steel. EC2 (1995) recommends values for E_s at high temperature for hot-rolled and cold-worked reinforcing steel, as shown in Table 2-2.

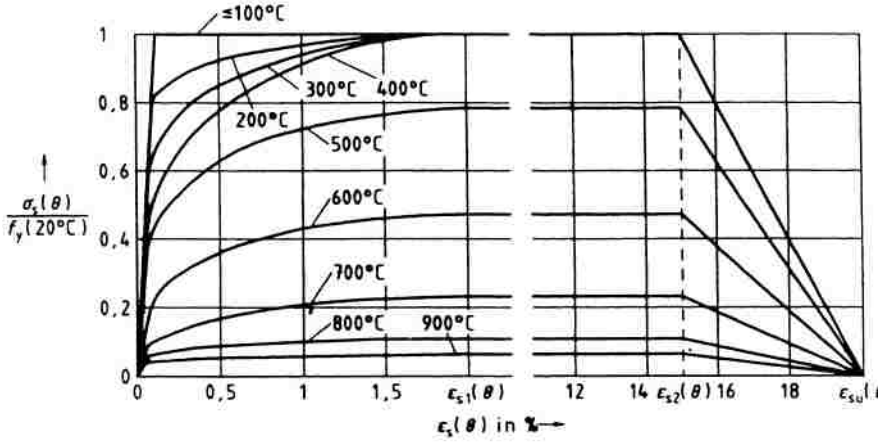

(a) Hot-rolled reinforcing steels

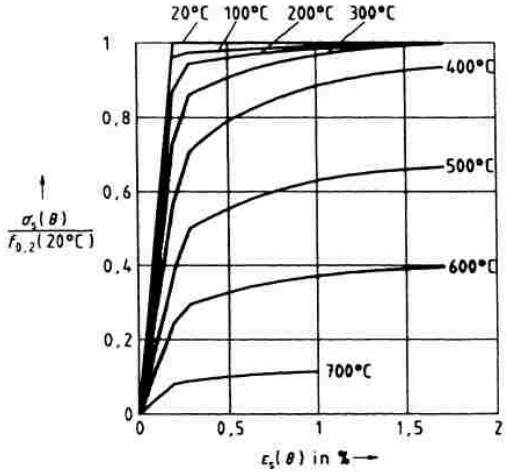

(b) Cold-worked reinforcing steels

Figure 2-17 Stress-strain response for reinforcing steel at elevated temperatures (European Committee for Standardization, 1995a)

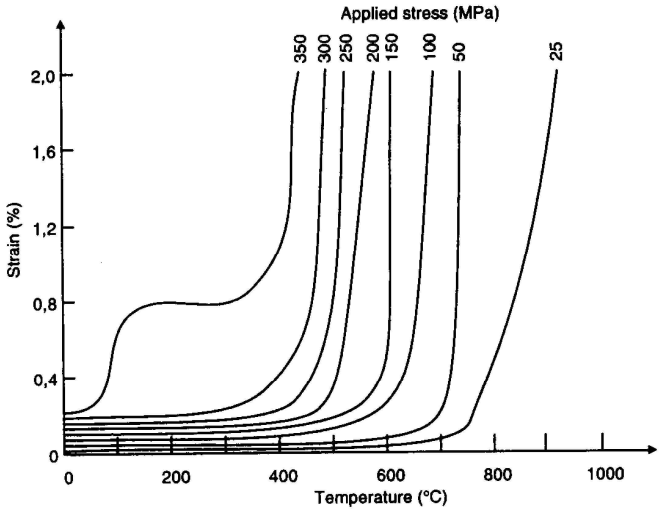

Figure 2-18 Creep of steel tested in tension (Kirby & Preston, 1988)

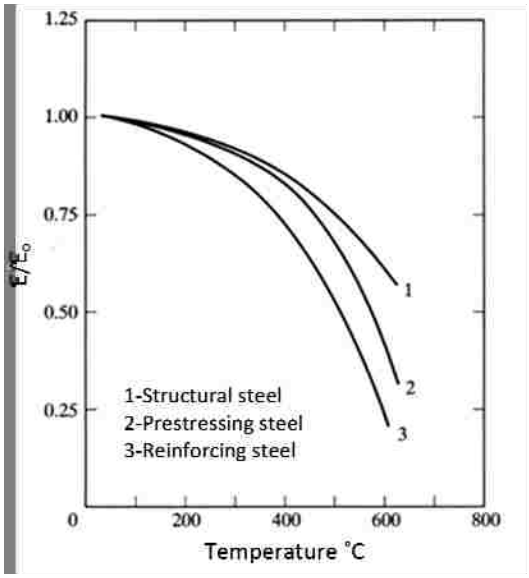

Figure 2-19 Variation of modulus of elasticity due to temperature (Harmathy, 1993)

Table 2-2 Modulus of elasticity at elevated temperature (European Committee for Standardization, 1995a)

Temperature (˚C)	Elastic Modulus of Reinforcing Steel (% of E_s)	
	Hot-rolled	Cold-worked
20	1	1
100	1	1
200	0.87	0.9
300	0.72	0.8
400	0.56	0.7
500	0.4	0.6
600	0.24	0.31
700	0.08	0.13
800	0.06	0.09
900	0.05	0.07
1000	0.03	0.04
1100	0.02	0.02
1200	0	0

2.7.7 Ultimate and Yield Strength

Attempts have been made to define effective yield strength of steel based on test data. However, the lack of a clear yield plateau of steel at higher temperatures leads to scattered definitions of yield strength as shown in Figure 2-20. Relative yield strength

defined as the ratio of yield strength at elevated temperature to that at ambient temperature is used in this figure. The dashed line shows the suggested yield strength for design purposes. Figure 2-20 also indicates that, compared with cold-worked steel, hot-rolled steel can better withstand high temperatures without significant reduction in ultimate and yield strengths. Some design codes define yield strength in slightly different ways from the dashed lines shown in Figure 2-20. Figure 2-21 shows the relative yield strength of hot-rolled and cold-worked reinforcement as specified by EC2 (1995).

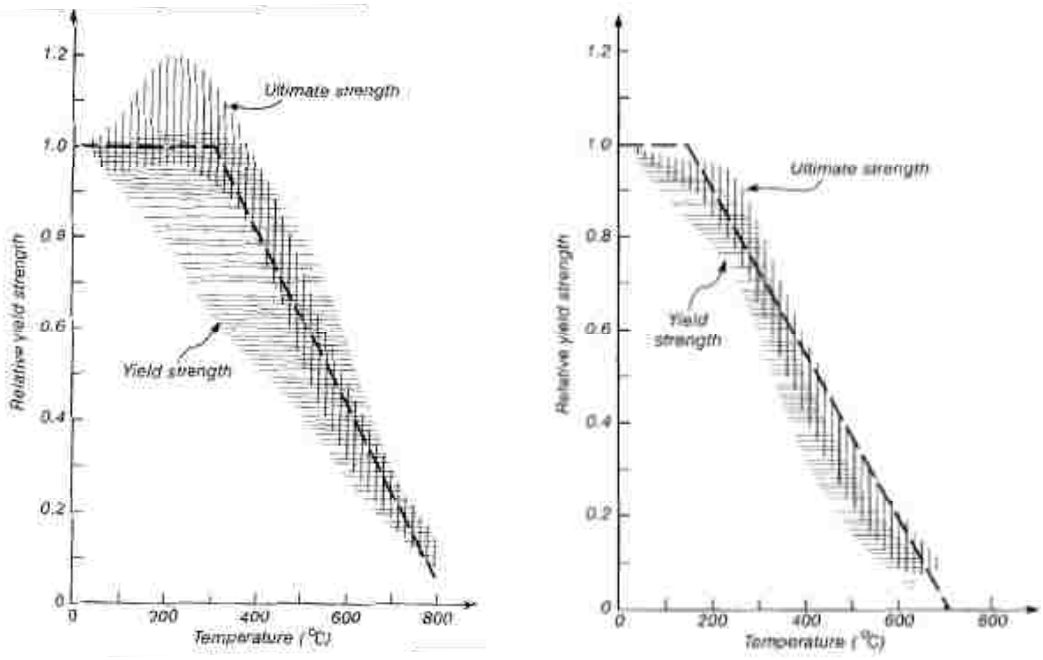

(a) Hot-rolled steel (b) Cold-worked steel

Figure 2-20 Ultimate and yield strength of steel (Harmathy, 1993)

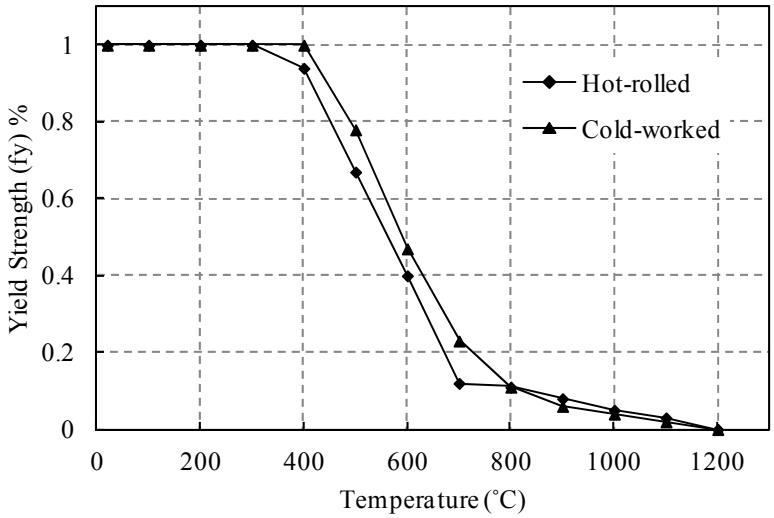

Figure 2-21 Design curves for reduction in yield strength of steel (European Committee for Standardization, 1995a)

2.8 Bond Strength of Concrete and Reinforcement

The bond between concrete and reinforcing steel is reduced as temperature increases. The degree of bond strength loss depends on the type of concrete and reinforcement (smooth or deformed). Measured bond strength is sensitive to testing method, but currently no standard test method exists. Bond strength is seldom considered critical. The underlying assumption is, when the bottom reinforcement is subjected to high temperatures under fire, the load is redistributed to the top reinforcement. The top bars at supports experience much lower temperature and thus are able to handle full bond stresses (Purkiss, 1996).

2.9 General Fire Resistance Requirements for Concrete Buildings

ASTM E119 requires that a member or system must obtain a specific hour rating. Within a desired time period, the member/system must "*Not suffer structural collapse, and if it functions as a barrier between two fire compartments, it must neither experience a temperature rise on the side away from fire of more than 250˚F (139˚C) as the average of several measurements, nor permit passage flame or hot gases through the floor or wall*

sufficient to ignite cotton waste that is held near the floor or wall" (Park & Gamble, 2000). The structural fire safety design is advancing toward performance-based approaches. However, the current design approach, established a century ago with little change, is prescriptive and widely recognized as inadequate (National Institute of Standards and Technology & United States, 2005).

2.9.1 Fire Resistance of Reinforced Concrete Slabs

The purpose of the aforementioned guidelines is to prevent the ignition of combustible material in contact with the unexposed surface. Fire tests indicated that heat transmission of a concrete slab depends on slab thickness and aggregate type (CRSI Committee of Fire Ratings, 1980). Figure 2-22 shows the experimentally determined slab thicknesses needed to satisfy the desired thermal endurance for various types of concrete commonly used in building construction. For normal weight concrete represented in this figure, aggregate size and air content were ¾ inch and 6%, respectively. For lightweight concretes, aggregate size was slightly less than ¾ inch and air content was around 7%. Each sample had a mid-depth relative humidity of 75% when the fire tests were performed.

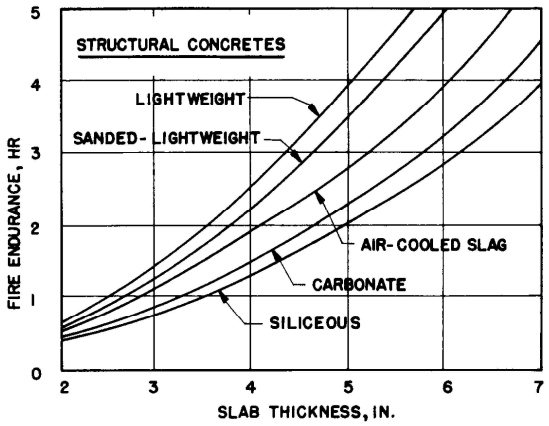

Figure 2-22 Fire endurance of slabs or walls based on heat transmission (CRSI Committee of Fire Ratings, 1980)

When a slab is subjected to a standard fire, the temperature distribution within the slab thickness is constantly changing (CRSI Committee of Fire Ratings, 1980). Figure 2-23 shows the test results for two types of concrete that were naturally dried and had a mid-depth relative humidity of 75% (Park & Gamble, 2000). From such test data, it is possible to predict concrete temperatures at given slab depths over a period of time. The CRSI (1980) states, "*in a slab exposed to fire from below, the average temperature of a reinforcing bar is approximately equal to the temperature of the concrete at the level of the center of the bar*." Thus, the graphs also allow a user to consider the degradation of steel properties when calculating the flexural capacity of a slab.

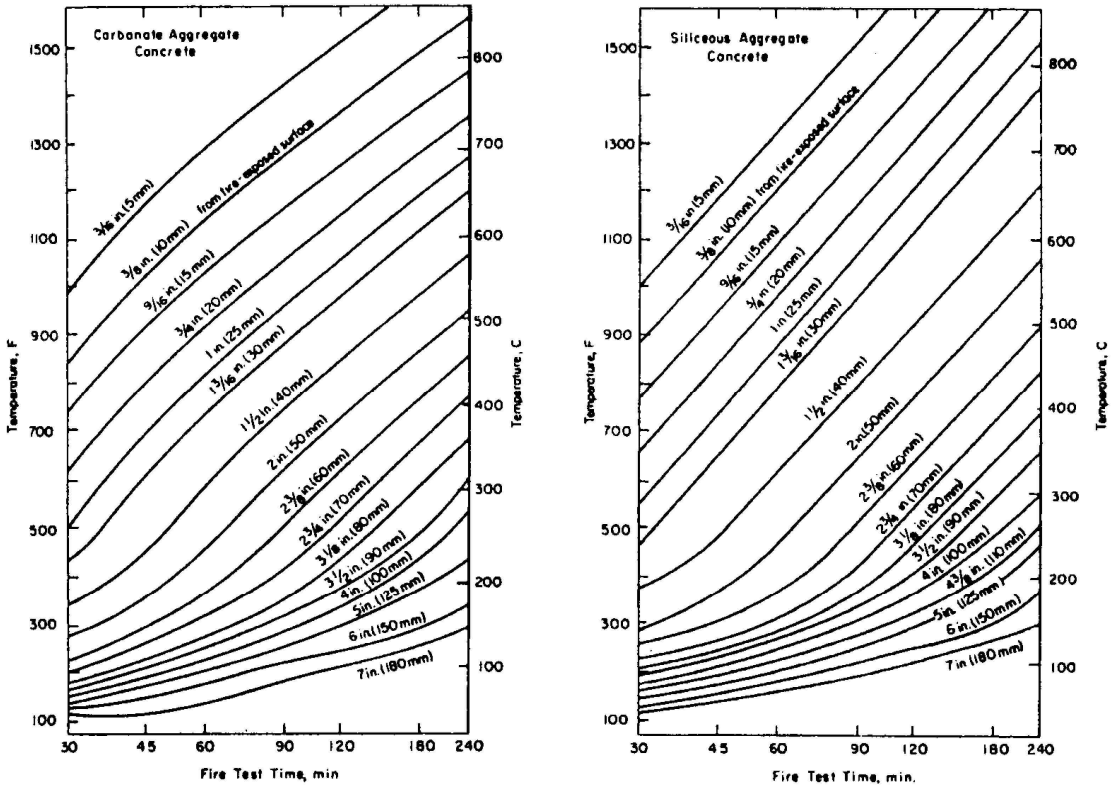

Figure 2-23 Temperatures within slabs during ASTM E 119 fire tests (ACI Committee 318, American Concrete Institute, & International Organization for Standardization, 2008; Joint ACI/TMS Committee 216, American Concrete Institute, & International Organization for Standardization, 2007).

Structural design recommendations for fire exposure are called generic or tabulated ratings (Buchanan, 2001). Table 2-3 and Table 2-4 show the minimum slab thickness and concrete cover required by ACI 216.1 (2007) to obtain a particular fire rating. Similar design criteria exist in other building codes such as EC2 (1995). Generic ratings for concrete slabs were developed by carrying out full-scale fire resistance tests using furnaces (Buchanan, 2001). Note that furnace tests are incapable of accounting for the two-way bending action existing in the slab and the in-plane restraint provided by slab supports (Moss et al., 2008). Therefore, the fire ratings for slabs derived from such tests are debatable.

Table 2-3 Fire resistance of single-layer concrete walls, floors, and roofs (Joint ACI/TMS Committee 216 et al., 2007)

Aggregate type	Minimum equivalent thickness for fire-resistance rating, inch.				
	1 hour	1.5 hours	2 hours	3 hours	4 hours
Siliceous	3.5	4.3	5.0	6.2	7.0
Carbonate	3.2	4.0	4.6	5.7	6.6
Semi-lightweight	2.7	3.3	3.8	4.6	5.4
Lightweight	2.5	3.1	3.6	4.4	5.1

Table 2-4 Minimum cover in concrete floors and roof slabs (Joint ACI/TMS Committee 216 et al., 2007)

Aggregate type	Cover for corresponding fire resistance (inch)					
	Restrained	Unrestrained				
	4 or less	1 hour	1.5 hours	2 hours	3 hours	4 hours
Nonprestressed						
Siliceous	3/4	3/4	3/4	1	1-1/4	1-5/8
Carbonate	3/4	3/4	3/4	3/4	1-1/4	1-1/4
Semi-lightweight	3/4	3/4	3/4	3/4	1-1/4	1-1/4
Lightweight	3/4	3/4	3/4	3/4	1-1/4	1-1/4
Prestressed						
Siliceous	3/4	1-1/8	1-1/2	1-3/4	2-3/8	2-3/4
Carbonate	3/4	1	1-3/8	1-5/8	2-1/8	2-1/4
Semi-lightweight	3/4	1	1-3/8	1-1/2	2	2-1/4
Lightweight	3/4	1	1-3/8	1-1/2	2	2-1/4

2.9.2 Fire Resistance of Reinforced Concrete Columns

Standard fire tests for concrete columns are much different from that for concrete slabs; slabs are heated from one side only, but columns are heated from all sides. Concrete columns generally perform well in fire because of a protected inner core due to the large size and the confinement provided by ties or spirals. Moreover, the reinforcing bars are usually protected by a minimum of 1-1/2 inches of concrete cover (CRSI Committee of Fire Ratings, 1980). Table 2-5 and Table 2-6 give the least dimension of concrete columns for specific fire-resistance ratings. These tables are applicable for columns with a concrete compressive strength of 12,000 psi or less. For concrete with compressive strength higher than 12,000 psi, the minimum column dimension required for all fire-resistance ratings is 24 inches (CRSI Committee of Fire Ratings, 1980).

Table 2-5 Minimum column size (Joint ACI/TMS Committee 216 et al., 2007)

Aggregate Type	Minimum column dimension for fire-resistance ranting, in.				
	1 hour	1-1/2 hours	2 hours	3 hours	4 hours
Carbonate	8	9	10	11	12
Siliceous	8	9	10	12	14
Semi-lightweight	8	8-1/2	9	10-1/2	12

Table 2-6 Minimum column size with fire exposure on two parallel sides (Joint ACI/TMS Committee 216 et al., 2007)

Aggregate Type	Minimum column dimension for fire-resistance ranting, in.				
	1 hour	1-1/2 hours	2 hours	3 hours	4 hours
Carbonate	8	8	8	8	10
Siliceous	8	8	8	8	10
Semi-lightweight	8	8	8	8	10

CHAPTER 3

CALIBRATION OF MODELING PARAMETERS FOR FINITE ELEMENT SIMULATIONS

3.1 FINITE ELEMENT SIMULATION OF FLAT-PLATES USING SHELL ELEMENTS

3.1.1 General Modeling Description

Finite element method is used in this research to estimate the slab local deformation demand near the column in flat plate structures subjected to combined gravity and fire-induced thermal loads. The analyses are performed using Abaqus (Dassault Systèmes Simulia Corporation, 2009), a general purpose finite element program. Abaqus is capable of simulating the behavior of typical engineering materials including metal, rubber, polymer, composite, reinforced concrete, crushable and resilient foam, and geotechnical materials such as soil and rock. Abaqus is chosen in this study as the simulation platform mainly for two reasons: First, when using shell elements for slabs, the flexural reinforcement can be conveniently modeled. Second, the reliability of the solvers for nonlinear analyses has been well acknowledged.

Although 3D solid elements can provide a more sophisticated simulation for slabs, it is deemed impractical for a system level analysis due to the high computational cost. For a flat plate structure, the span-to-thickness ratio of slab is normally larger than 30. Shell elements, applicable for modeling components in which one dimension is significantly smaller than the others, are therefore adopted in this study to model slabs. Figure 3-1 shows the idealization of a thin structural component into conventional shell elements. The shell geometry is defined at a reference surface and thickness is specified as one of the sectional properties. Each node of a shell element contains three displacement and three rotational degrees of freedom.

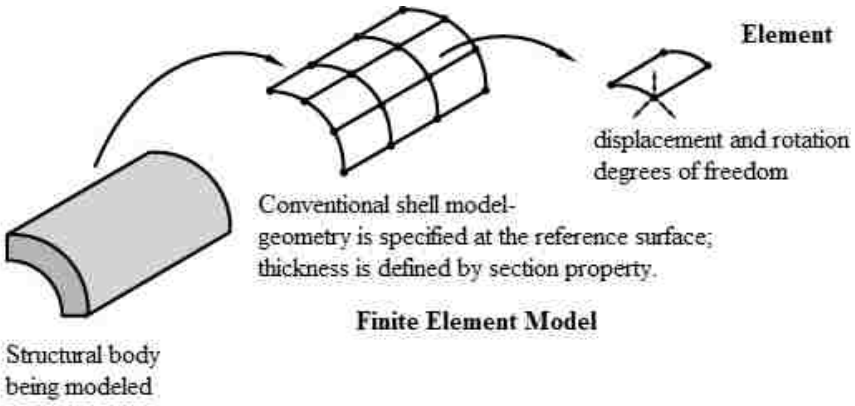

Figure 3-1 Modeling thin components using shell elements (Dassault Systèmes Simulia Corporation, 2009)

The deflection of a concrete slab, especially after cracking, is dominated by flexure, and the effects of shear on slab deformation are negligible. Thus, the thin shell element S4R available in Abaqus, a type of 4-node shell element with reduced integration, is used in this study. Simpson's rule is adopted for integration at a section to evaluate the slab internal forces. Thirteen integration points are defined at a section. Temperature variation through the thickness of slab is assumed to be piecewise quadratic.

The slab flexural reinforcement is modeled using the *Rebar Layer* option in Abaqus. The reinforcement is considered as one-dimensional material resisting axial force only. The rebar size, spacing, location, and orientation are defined as sectional properties of shell elements in the analyses.

3.1.2 Material Modeling

The mechanical and thermal properties of concrete and steel have been discussed previously in Chapter 2. These properties are defined as a function of temperature according to the formulations suggested by design codes or previous studies. The following summarizes how concrete and steel are modeled in the analyses.

3.1.2.1 Concrete

The mass density of concrete can be expected to stay roughly the same even at high temperatures, although a small reduction can be considered at or above 100˚C to account for the evaporation of free water. In this study it is assumed that normal weight concrete, siliceous or calcareous, has a constant mass density of 2300 kg/m^3 (European Committee for Standardization, 1995a).

Elastic properties, including Poisson's ratio and modulus of elasticity, need to be specified in the analyses. Because little is known about Poisson's ratio at high temperatures, the Poisson's ratio of concrete is defined as 0.2, a value commonly used for concrete at ambient temperatures. At ambient temperature, the modulus of elasticity is defined E_c (psi) as:

$$E_c = 57000 \times \sqrt{f_c} \qquad \text{Equation 3-1}$$

Equations 2-17 and 2-18 suggested by EC2 (1995) are used to define the concrete modulus of elasticity as a function of temperature.

The *Concrete Damage Plasticity* (CDP) is employed to model slab concrete. This model is applicable to quasi-brittle materials subjected to monotonic, cyclic, and/or dynamic loading. It assumes two main failure mechanisms: compressive crushing and tensile cracking. To apply this model, the concrete properties under uniaxial loading are defined in this study following EC2's (1995) recommendation (Figure 3-2). The uniaxial properties are then converted by the program, according to the CDP model, to the constitutive behavior of concrete under tri-axial state of stresses (Dassault Systèmes Simulia Corporation, 2009).

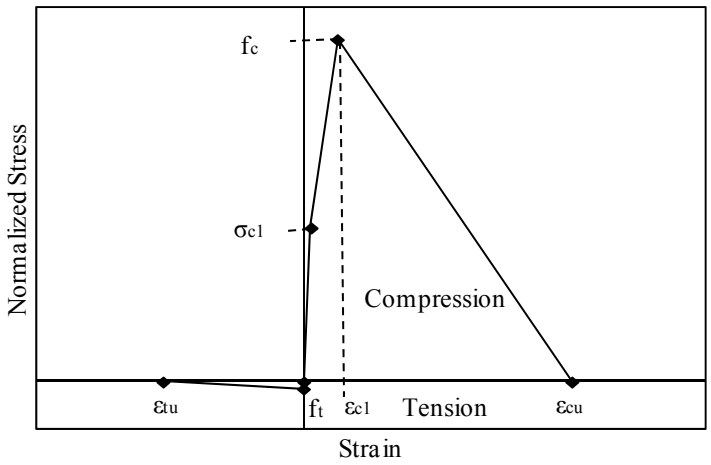

Figure 3-2 Uniaxial loading response for using *Concrete Damage Plasticity* model

Figure 3-2 graphically represents the stress-strain model used in analyses. Concrete under compression behaves linearly with a slope of E_c until reaching a stress of σ_{c1} (σ_{c1} = 0.45f_c), after which the material experiences strain hardening. Once the peak stress (f_c) is reached, strain softening is initiated. Strain values ε_{c1} and ε_{cu} at elevated temperatures are given by EC2 (1995) in Table 2-1. A bilinear response with strength degradation is assumed for concrete in tension. The failure stress of concrete in tension, f_t, represents the onset of micro-cracking. Note that f_t is generally less than f_r, the concrete flexural tensile strength specified in design codes. Beyond f_t, the stress-strain curve softens to reflect the formation of micro-cracks and further reaches zero stress at ε_{tu}. The definition of f_t and ε_{tu} will be calibrated from test data, as discussed in Section 3.2.1.

Figure 3-3 models normalized stress, the ratio of stress at elevated temperature to the concrete compressive strength at room temperature, used in the analyses. It should be noted that concrete tensile strength vanishes when temperature reaches 600ºC as shown in Figure 2-16.

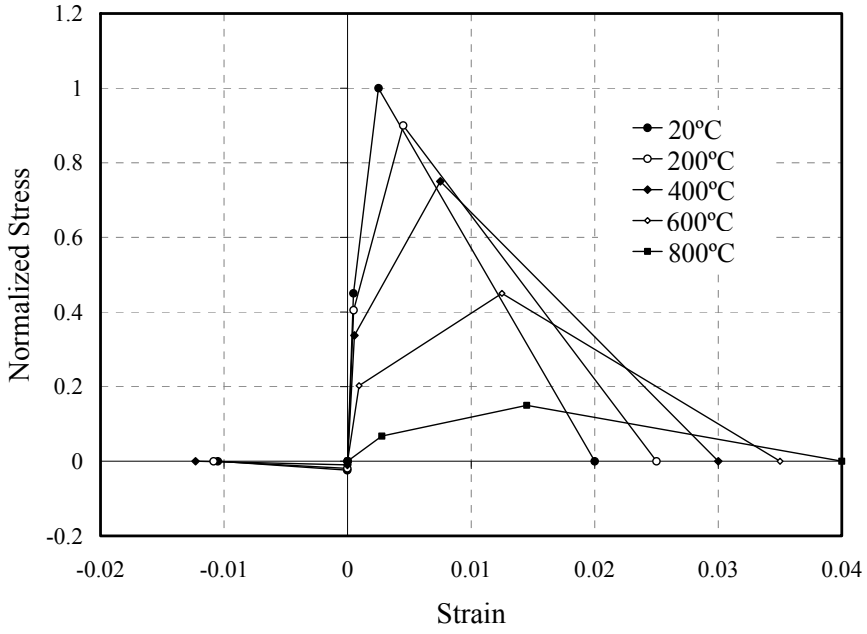

Figure 3-3 Normalized stress-strain curve at high temperature

In addition to the uniaxial tensile and compressive behavior, five other parameters must be defined in order to use the *Concrete Damage Plasticity* model:

(1) Dilation angle (ψ) represents the ratio of plastic volume change over plastic shear strain. It is found to be constant near and at concrete compressive strength. In the theory of associated plasticity, ψ is often assumed equal to the friction angle. For concrete, the friction angle was reported with a value between 30˚ and 35˚ (Vermeer & De Borst, 1984). However, Vermeer (1984) suggested a non-associated plasticity for concrete where the dilation angle be defined with a value between 0˚ and 20˚. Due to relative large range of this suggested value, the appropriate value of dilation angle for use in the analyses of flat plates is to be calibrated from test data (Section 3.2.1).

(2) The flow potential eccentricity defines the rate at which the flow potential function approaches the asymptote. If a material has approximately the same

dilation angle over a wide range of confining pressures, the value of flow potential eccentricity is equal to 0.1. Because the dilatancy of concrete is constant before and beyond peak strength and is known to vanish at high confining pressure (Vermeer & De Borst, 1984), a flow potential eccentricity equal to 0.1 is used in this study.

(3) The ratio of initial equibiaxial compressive yield stress to initial uniaxial compressive yield stress ranges narrowly from 1.10 to 1.16 as suggested by Lubliner et al. (1989). A value of 1.16 is chosen for the model.

(4) The ratio of the second stress invariant on the tensile meridian to that on the compressive meridian is defined as 0.667 based on experimental evidence (Lubliner, Oliver, Oller, & Oñate, 1989).

(5) The viscosity parameter can be used to overcome convergence difficulties when the material experiences stiffness degradation. A low viscosity value helps improve the convergence rate without compromising accuracy. A zero value of the viscosity parameter is used in this study so that no viscoplastic regulation is enforced (Dassault Systèmes Simulia Corporation, 2009).

Conductivity, specific heat, and thermal expansion of concrete must also be defined for the analyses of reinforced concrete structural assemblies at elevated temperatures. Due to the discrepancies in their definitions given by different sources, as discussed in Sections 2.4.1, 2.4.2, and 2.4.3, these properties require further calibration. The appropriate definitions for conductivity and specific heat will be calibrated in Section 3.2.2, and the definition for thermal expansion will be calibrated in Section 3.2.3.

3.1.2.2 Steel Reinforcement

The mass density of steel essentially remains unchanged at high temperatures. A density of 7850 kg/m^3 is defined in this study for reinforcing bars. The modulus of elasticity, E_s, is defined as 29000 ksi (2.0×10^5 MPa) at ambient temperature. At higher temperature, E_s is defined according to EC2 (1995) as shown in Table 2-2. The Poisson's ratio of steel reinforcement is taken as 0.3 and assumed to be constant at different temperatures. Steel reinforcement is modeled as a uniaxial material with a bilinear stress-strain relationship for both tension and compression. The yield stress of reinforcement at elevated temperatures is defined in accordance with Figure 2-21 (Section 2.7.7). The strain hardening ratio beyond yielding is assumed to be 1% of E_s at ambient temperature. To ensure convergence, no strain hardening beyond yielding is considered for elevated temperature.

The thermal expansion of reinforcement is defined based on the linear approximation of $\varepsilon_{th} = 14 \times 10^{-6}(T - 20)$ (European Committee for Standardization, 1995a). Due to software limitation, the specific heat and conductivity of reinforcement are not included in the heat transfer analysis. Nevertheless, the effects of these properties, as discussed by Wang (2006), are expected to be negligible. In Wang's study, a 2-D heat transfer analysis was conducted on a slab subjected to elevated temperature using finite element program SAFIR. The slab was 200 mm thick and reinforced with 10 mm square bars located 30 mm from the slab bottom surface. The thermal load, a standard fire without decay phase, was applied below the slab and the heat transfer analyses were performed for two cases: with and without considering the reinforcing bars. Table 3-1 gives the predicted slab temperature at the location of reinforcement. The maximum difference in concrete

temperatures between the two cases was less than 8˚C. It can therefore be assumed that the absence of reinforcing bars in the analysis does not significantly affect the heat transfer through slab.

Table 3-1 Comparison of temperatures of concrete with and without considering reinforcing bars in heat transfer analysis (Wang, 2006)

Time (min.)	Temperature (˚C)			
	Reinforcing bars	Concrete with reinforcing bars	Concrete without reinforcing bars	Difference in concrete temperature
60	403	407	402	5
120	593	595	588	7
180	702	705	697	8
240	779	782	775	7

3.2 Calibration of Modeling Parameters from Test Data

In order to minimize the uncertainty involved in the system level simulation of flat plates subjected to elevated temperature, the key parameters for finite element modeling are calibrated with the data of experiments performed at component level. For this purpose, analyses are conducted on the test specimens subjected to three different loading conditions:

- Gravity loading of isolated slab-column connections in ambient temperature
- Thermal loading of slabs without applying gravity loads
- Combined gravity loading and thermal loading of two-way slabs

3.2.1 Calibration of Mechanical Modeling Parameters from Static Loading Tests

Simulations are made on isolated slab-column connections to calibrate the appropriate mesh size of shell elements, dilation ratio needed to define the *Concrete Damage Plasticity* model, and uniaxial tension behavior of concrete. Two tests (B-2 and B-4)

conducted by Elstner and Hognestad (1956) are simulated because the specimens had slab tensile reinforcement ratios (ρ = 0.50 and 0.99% for B-2 and B-4, respectively) representative of practical applications. Figure 3-4 and Table 3-2 summarize the specimen geometry, material properties, and loading condition. The tensile reinforcing bars were uniformly distributed in the slabs. Neither compressive reinforcement nor shear reinforcement was used. During the test, the slab was placed up-side-down and simply supported at four edges. However, the corners of the slab were permitted to lift up. A vertical load used to simulate the effects of gravity loading was applied at the center column stub, where the slab deflection was measured.

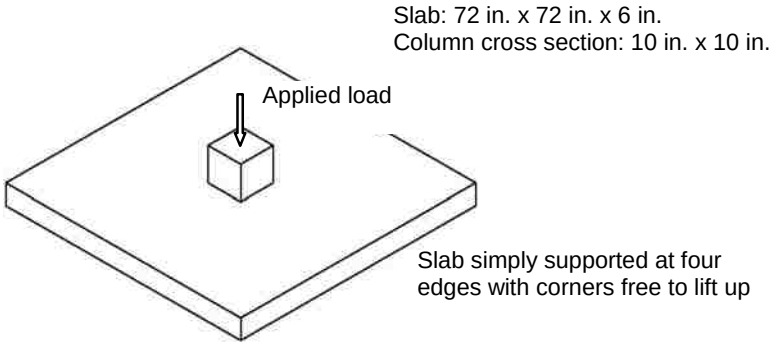

Figure 3-4 Test set-up for specimens subjected to concentric gravity loading

Table 3-2 Outline of Test Specimen Properties

Slab	Concrete Strength (psi)	Tension Mat				
		Bar Size	Spacing (in.)		Reinforcement ratio, ρ(%)	f_y (ksi)
			Bottom	Top		
B-2	6900	No.4	9.375	8.375	0.50	46.5
B-4	6920	No.5	7.375	6.375	0.99	44.0

In the analyses, the nonlinear material models for concrete and steel at ambient temperature described previously are applied to the slabs. Elastic material properties with large stiffness are assigned to the slab-column joint regions. Displacement-driven

analysis is performed on each specimen by specifying a target center displacement at slab-column joint beyond the displacement where first yield was observed in the tests.

A sensitivity study is conducted by performing analyses of the specimens using three different mesh sizes while using the same modeling approach for the other parameters (ψ= 15˚, f_t = 20% of concrete rupture strength). Figure 3-5 shows the analysis results in terms of load-center deflection response using small, medium, and large mesh size corresponding to 0.5, 1.0, and 1.5 times the slab thickness, respectively. It is seen that the results are almost identical until the slabs reach a deflection of 0.1 in. (elastic range), after which the response evaluated using the medium mesh size is very close to that using the small mesh size. Additionally, when using the smallest mesh size, convergence problems become severe at large deformations. Thus, mesh size equal to or less than the slab thickness is chosen for all the other analyses in this study to achieve efficient calculations, avoid convergence trouble, and maintain sufficient accuracy.

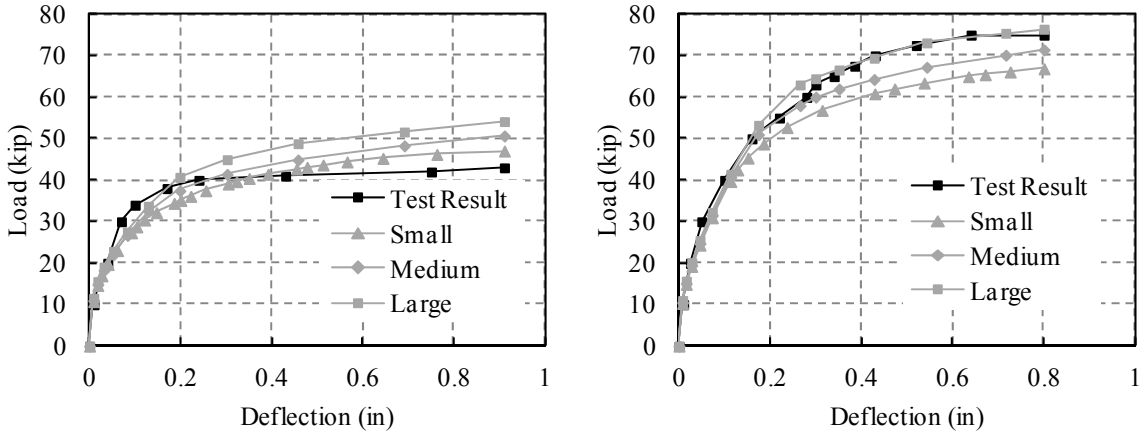

(a) Specimen B-2 (b) Specimen B-4

Figure 3-5 Effect of mesh size on calculated load-deflection response

Several types of stress-strain relations for concrete in tension have been proposed, but no consensus has been reached. EC2 (1995) suggests neglecting concrete tensile strength because it is conservative for design purposes. This approach has also been adopted in

most numerical simulations, such as those by Lim et al. (2004) and Moss et al. (2008). A simplified bilinear tension model shown in Figure 3-6 is used herein to ensure converged results and avoid significantly underestimated stiffness of slabs. The peak tensile stress $f_t = x_1 f_r$ is defined as a fraction of the concrete modulus of rupture, f_r, given in Equation 2-20. Following the reach of f_t, concrete experiences strain softening and stress reduces to zero at a strain of $\varepsilon_{tu} = x_2 \varepsilon_t$, where $\varepsilon_t = \frac{f_c}{E_c}$.

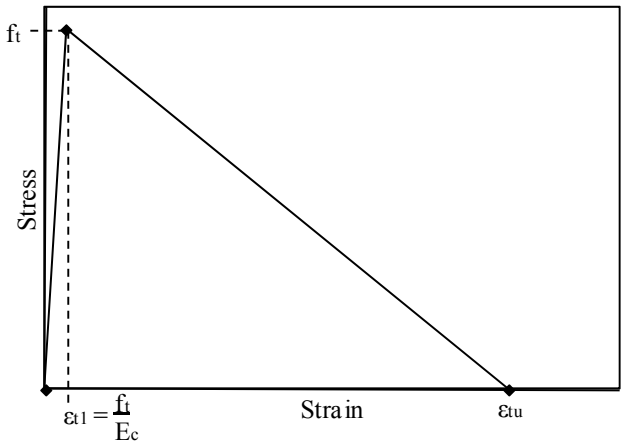

Figure 3-6 Simplified Model for Concrete in Tension

Ghaffar et al. (2005) adopted x_1 as 0.3. Nilson et al. (2003) defined the direct concrete tensile strength to be between $3\sqrt{f'_c}$ psi ($0.4f_r$) and $5\sqrt{f'_c}$ psi ($0.66f_r$) for normal weight concrete. Note that the values of x_1 and x_2 greatly affect the convergence of an analysis if sharp strength degradation exists. Several combinations of x_1 and x_2 are examined based on the recommendations by other researchers and the ability to obtain converged results that reasonably predict the strength of slab-column assemblies. A large x_2 value is often associated with overestimated strength, while a low value leads to serious convergence problems. Based on this consideration, a final value of $x_2 = 10$ is chosen.

Figure 3-7 shows the analysis results using two combinations (x_1 = 0.3 and x_2 = 10, x_1 = 0.2 and x_2 = 10) that predict load-center deflection response similar to test results. ψ = 15˚ is used in the analyses. It is seen that the combination of x_1 = 0.2 (f_t = 0.2f_r) and x_2 = 10 (ε_{tu} = 10ε_t) results in slightly better simulation for the two specimens and is thus used for the further analyses.

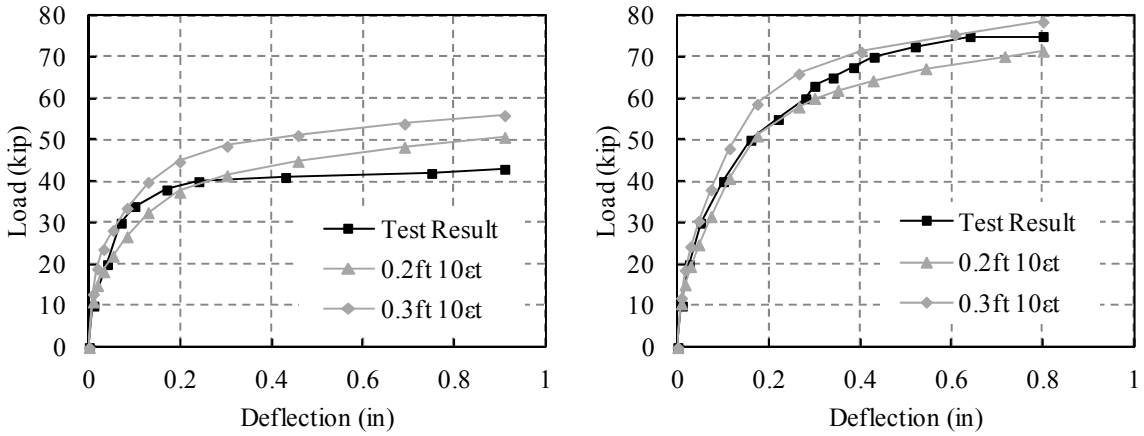

(a) Specimen B-2 (b) Specimen B-4

Figure 3-7 Effect of concrete tensile behavior on calculated load-deflection response

The effects of dilation ratio (ψ) are examined. The calibration results obtained earlier for mesh size and concrete tensile behavior are adopted in the modeling. Figure 3-8 compares the analysis results for the two specimens using two different values of dilation ratio, ψ = 15° and 30°. These values are chosen for the associated and non-associated plasticity theories presented in Section 3.1.2.1. It is found that discrepancy exists only if the specimens are loaded to relatively large deflections. However, the difference is not significant and thus a value of ψ = 15° is chosen for further analyses.

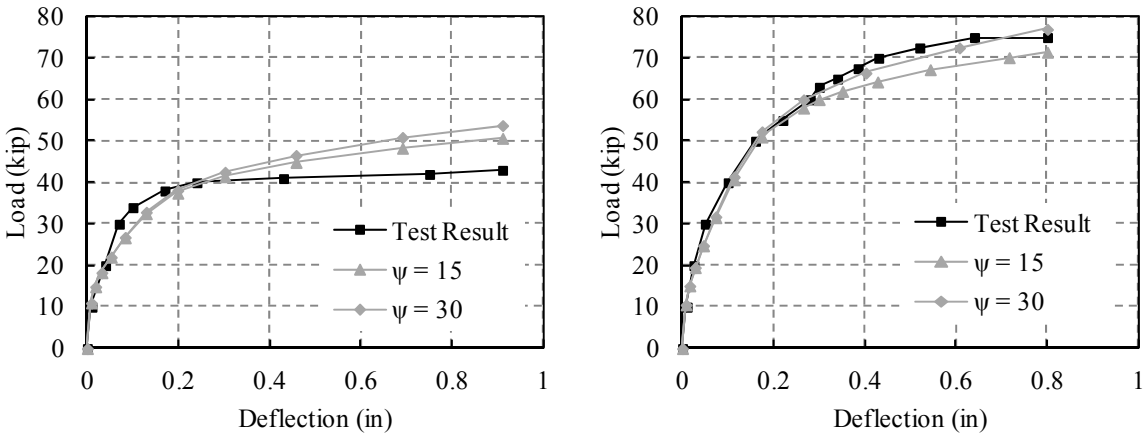

(a) Specimen B-2 (c) Specimen B-4

Figure 3-8 Effect of dilation ratio on calculated load-deflection response

The following summarizes the results of analyses based on the modeling parameters already calibrated. Figure 3-9 shows the plan view of the slab deflection in Specimen B-2 when it is loaded to a center deflection of 0.91 in. Deflection is greatest around the column and decreases to zero at the supports. Figure 3-10 compares the predicted and measured load-deflection responses for the two specimens. Good agreement is achieved between the simulation and test results for Specimen B-4. The predicted strength of Specimen B-2 is about 15% higher than the measured value. This discrepancy is deemed acceptable given the many modeling parameters involved in defining the nonlinear response of concrete.

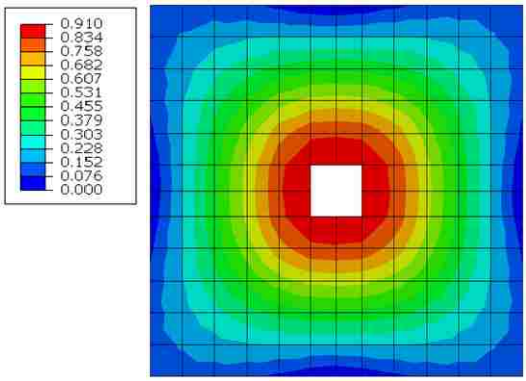

Figure 3-9 Calculated slab deflection for Specimen B-2 (unit: inch)

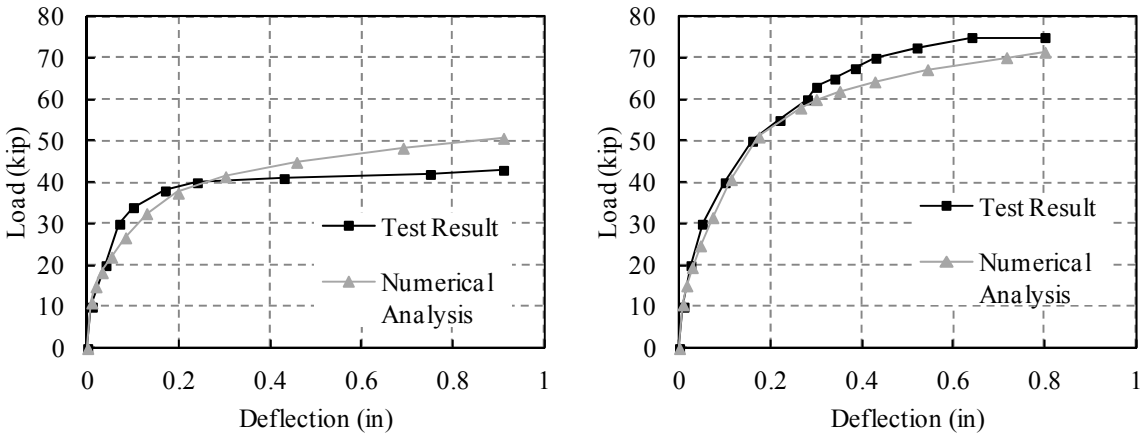

(a) Specimen B-2 (b) Specimen B-4

Figure 3-10 Comparison of measured and predicted load-deflection response

To further validate the finite element modeling, the predicted local behaviors of slabs are examined in terms of their sectional rotation and rebar force at large deformation. The performance of Specimen B-2 predicted from finite element simulation is described as an example. Figure 3-11a shows the plan view of section rotation at the largest slab center deflection (0.91 in.) applied to Specimen B-2. Along the slab center line, fairly small difference exists in slab rotation at sections outside the vicinity of column. This indicates that, at large deformations, slab deforms mainly by rigid body rotation due to the highly localized deformation near the column caused by concrete cracking and reinforcement yielding. The situation can be clearly demonstrated by Figure 3-11b, which shows the section rotation about Y-axis for half of the specimen (cut along a slab center line) at its deformed position. Such deformation characteristics obtained from analysis is consistent with that observed in the tests by Guandalini et al. (2009) (Figure 2-2).

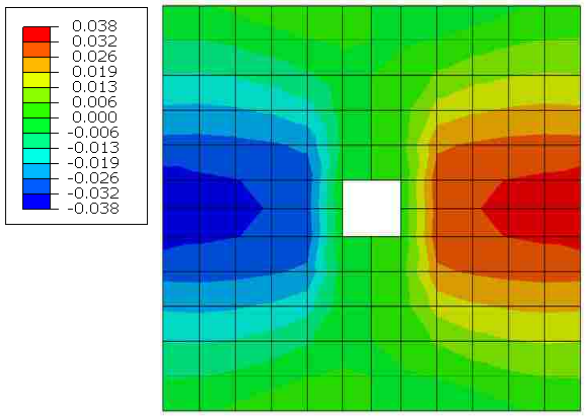

(a) Plan View

(b) 3D view of half slab

Figure 3-11 Slab Rotation for Specimen B-2 (unit: radian)

Figure 3-12 shows the force in slab tensile reinforcement oriented in two orthogonal directions for Specimen B-2 when it has been loaded to a center deflection of 0.91 in. Based on the reported material properties, the rebar had a yield force of 9.1 kips. According to this yield force, the red color in Figure 3-11 indicates the location of reinforcement that are yielded or close to yielding. The highest stressed reinforcement is always located at the column face. The yielding pattern identified from finite element simulations is compared with the yield lines (Figure 3-13a) derived from yield line theory (Hognestad, 1953) The yield lines develop at slab-column interface and extend from column corners to slab edges at points located 17.6 in. from slab corners. Although yield lines are not completely generated in analyses, the yielding of rebar has extended to a large region of the slab and followed a pattern consistent with the theoretical yield lines. The yielding pattern shown in Figure 3-12 is also consistent with the distribution of the

widely opened slab cracks radiated from column to slab edges as shown in Figure 3-13b (Elstner & Hognestad, 1956).

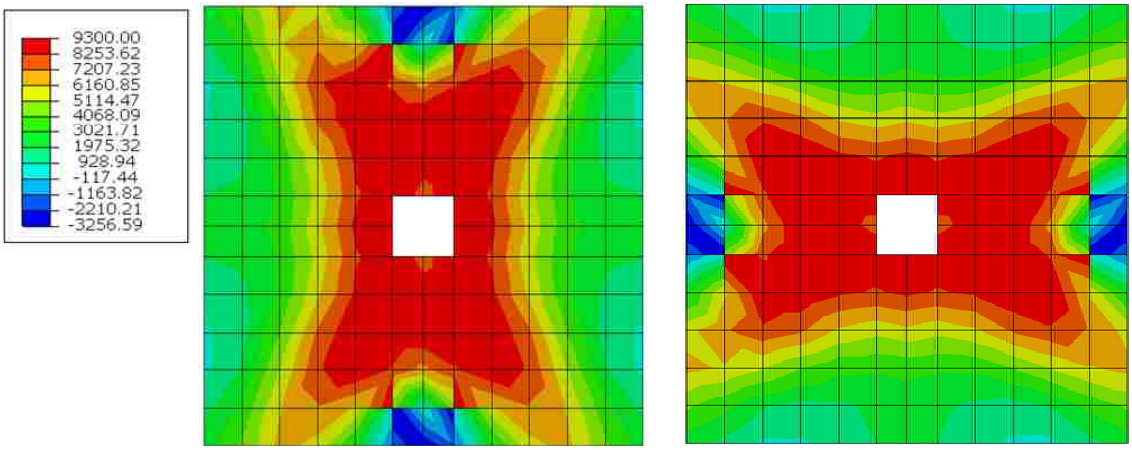

(a) Force of rebar in X-direction (b) Force of rebar in Y-direction

Figure 3-12 Rebar force (unit: lb)

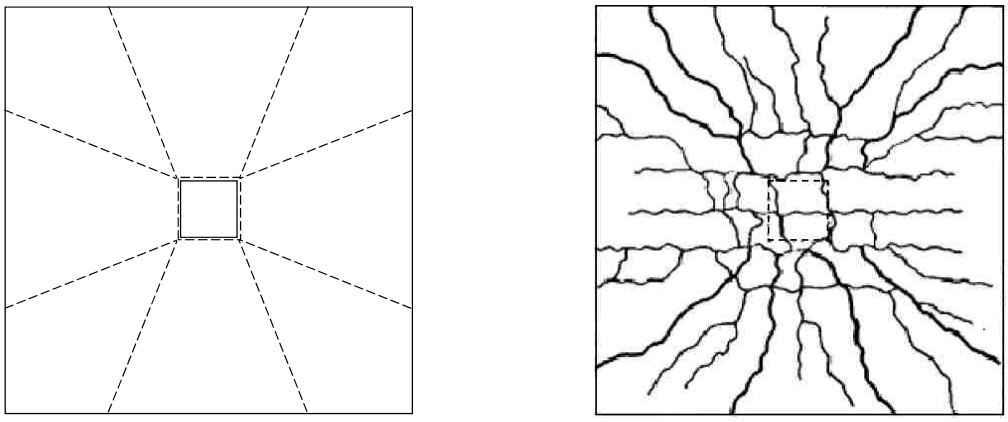

(a) (b)

Figure 3-13 Yield line and typical crack pattern (Elstner & Hognestad, 1956)

3.2.2 Calibrating Conductivity and Specific Heat of Concrete

The definitions of conductivity and specific heat of concrete recommended by EC2 (1995) and Lie (1992) (Section 2.4.1 and Section 2.4.2) are examined by carrying out heat transfer simulation for Specimen HD12, one of the three specimens tested by Lim

and Wade (2002). All these specimens were 3.3-m wide, 4.3-m long, and 100-mm thick slabs constructed using siliceous concrete with nearly identical compressive strength. The type and amount of flexural reinforcement varied among the specimens. Table 3-3 gives the detailed properties of these specimens. In the tests, the slabs were simply supported at the four edges. The corners of Specimens 661 and HD12 were unrestrained from vertical displacement, while the corners of Specimen D147 were clamped down because unrealistic curling of the slab occurred in earlier tests. Figure 3-14 shows the test setup for the specimens. In each test, a constant gravity load of 5.4 kPa was first applied by steel water drums and followed by a three-hour ISO 834 standard fire applied below the slab by a furnace. The water drums were prevented from tipping as the slab deflected during thermal loading. Slab deflections were measured at several locations in the tests.

Table 3-3 Outline of Lim and Wade (2002) tests

Slab	Total Load (kPa)	Concrete Strength (MPa)	Reinforcement	Reinforcement Diameter (mm)	Reinforcement Spacing (mm)	f_y (MPa)
D147	5.4	36.6	cold-worked deformed	8.7	300	565
661	5.4	36.6	cold-worked plain	7.5	150	568
HD12	5.4	36.7	hot-rolled deformed	12	200	468

Figure 3-14 Fire testing of slabs (Lim & Wade, 2002)

As mentioned earlier, heat transfer of a reinforced concrete slab is largely unaffected by the presence of reinforcement. Therefore, slab reinforcement is not incorporated into this type of analysis. For the same reason, only Specimen HD12 is used to calibrate the thermal properties of concrete. Note that heat transfer is independent to the stress condition of the material. Thus, the gravity loads applied on the slabs in the tests are not considered. Even though all the tests utilized ISO 834 standard fire, the actual atmosphere temperature near the slab was different. The time-temperature histories measured at slab bottom surface in the tests are applied at this location in analyses to obtain meaningful results.

It can be assumed that heat transfers at a constant rate through the concrete slab. Therefore, the identical slab thickness shall produce similar heat transfer results over the entire slab. The temperatures determined from analyses are compared with those measured from Specimen HD12 at several locations along the slab depth. Figure 3-15 shows a group of time-temperature curves, each corresponding to the temperature at a certain distance from the slab bottom (heated surface).

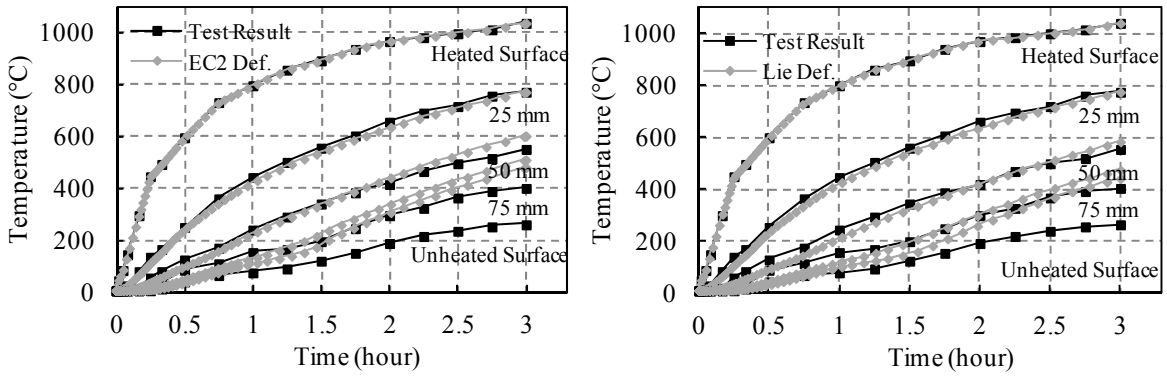

Figure 3-15 Comparison of calculated and measured temperatures for Lim and Wade (2002)

Figure 3-15 indiactes that the thermal properties of concrete defined by EC2 (1995) and Lie (1992) predict the measured temperature of slab within 75mm from the heated

surface fairly well. Beyond this region, the slab temperature is overestimated. Note that the bottom reinforcement in actual slabs normally has a clear cover equal to or slightly higher than 0.75 in. (19 mm). furthermore, the concrete depth underneath the tip of inclined shear crack immediately prior to punching failure can be much less than slab thickness (Y. Tian, 2007). Thus, the thermal properties given by EC2 (1995) and Lie (1992) can reasonably estimate the temperature of slab in the critical regions. Because Lie's model (1992) for conductivity and specific heat of concrete results in slightly better predictions than EC2 (1995), this model is adopted in the followling analyses.

3.2.3 Calibrating Thermal Expansion of Concrete

Finite element simulations are performed on all three slabs (D147, HD12, and 661) tested by Lim and Wade (2002) to calibrate the definition of thermal expansion of concrete. The simulation for each test contains two steps. In the first step, heat transfer analysis using Lie's formulation (1992) for conductivity and specific heat of concrete is conducted by applying the actual time-temperature histories at slab bottom in the analyses. In this step, the mechanical properties of concrete and steel under elevated temperature defined in Section 3.1.2 are employed; vertical loads simulating the gravity loading in the tests are applied at room temperature; and then the slab temperature gradient determined from the first step is applied. The definitions of concrete thermal expansion given by EC2 (1995) and Lie (1992) (Section 2.4.3) are individually examined by analyses. Figure 3-16 shows the comparison of predicted and measured slab center deflections for the three tests.

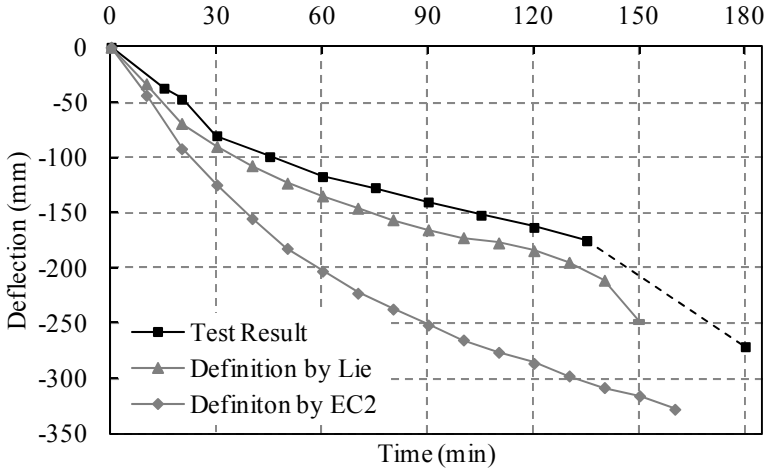

(a) Specimen D147

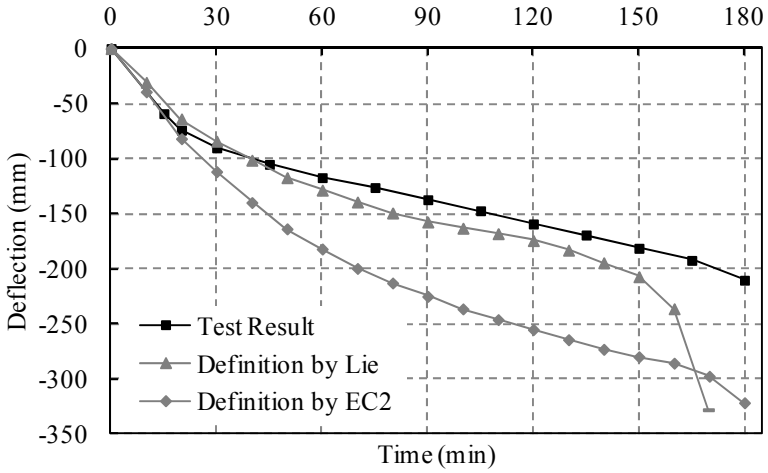

(b) Specimen 661

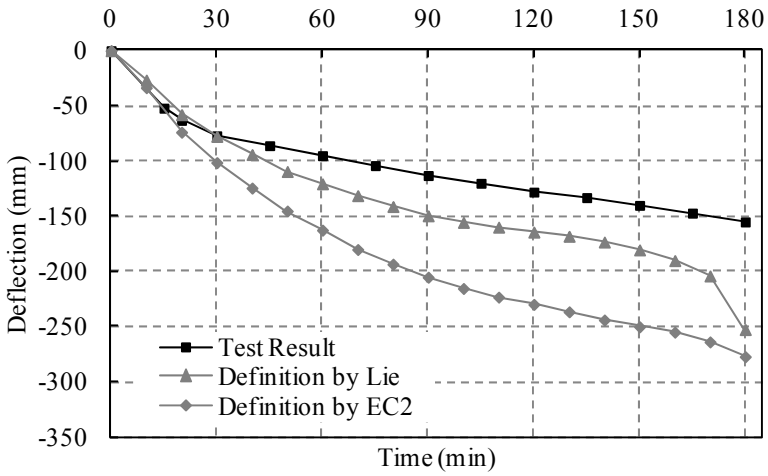

(c) Specimen HD12

Figure 3-16 Comparison of calculated and measured slab center deflection for three tests

It is seen from Figure 3-16 that the best agreement between the test result and simulation based on Lie's formulation is achieved in Specimen 661. For Specimens D147 and HD12, finite element simulation using Lie's (1992) model overestimates the slab center deflection at t = 90 minutes by 15% and 25%, respectively. During testing Specimen D147, the rotary potentiometer used to measure slab center deflection failed at t = 135 minutes due to excessive slab deflection. A final deflection, shown by the ending point of the dashed line in Figure 3-16a, had to be measured again after the test was completed. Note that, for this specimen, analysis successfully predicts the heating time when the slab deflection rapidly increased in the test, which likely announced the onset of failure.

In general, Lie's (1992) definition of thermal expansion leads to better predictions than that of EC2 (1995), especially for Specimens D147 and 661. It is obvious that, for this series of test, the definition of concrete thermal expansion given by EC2 (1995) results in significantly underestimated slab stiffness under elevated temperature. As a result, Lie's formulation of concrete thermal expansion is adopted in this study.

CHAPTER 4

PERFORMANCE OF A FLAT PLATE BUILDING SUBJECTED TO FIRE

4.1 PROTOTYPE STRUCTURE

The prototype flat plate structure, as shown in Figure 4-1, is a four story office building designed with 1.5 hour fire resistance. The building has a 10 ft. (3.05 m) story height and four bays in each direction spanning 20 ft. (6.1 m) between column centers. It is assumed that gravity loads control the design. Consequently, no lateral load systems such as perimeter moment frames or shear walls are employed. The design of this prototype structure follows the building design codes ASCE 07-10 (2010), ACI 318-08 (2008), and ACI 216.1-07 (2007). The design gravity loads on each floor consist of slab self-weight plus 30 psf (1.44 kN/m^2) superimposed dead load and 50 psf (2.39 kN/m^2) live load. The slabs are supported on 15 in. (381 mm) square columns without using shear capitals or drop panels. Grade 60 hot-rolled reinforcement (f_y = 60 ksi (414 MPa)) and normal weight concrete with a cylinder compressive strength of 4000 psi (27.6 MPa) are used to construct the slabs and columns. The concrete is made of siliceous aggregates with 3/8 in. (9.53 mm) maximum size.

Because the building has a regular floor plan and more than three bays in each direction, the *Direct Design Method* provided in ACI 318-08 (2008) is used to design the slabs. The slab thickness is chosen as 7.5 in. (190.5 mm) to satisfy the code requirements regarding deflection serviceability and two-way shear strength. The clear cover of slab flexural reinforcement is 3/4 in. (19.1 mm). The slab thickness and the size of concrete cover satisfy the ACI 216.1-07 (2007) requirements for 1.5 hour fire resistance as shown in Table 2-3 and Table 2-4.

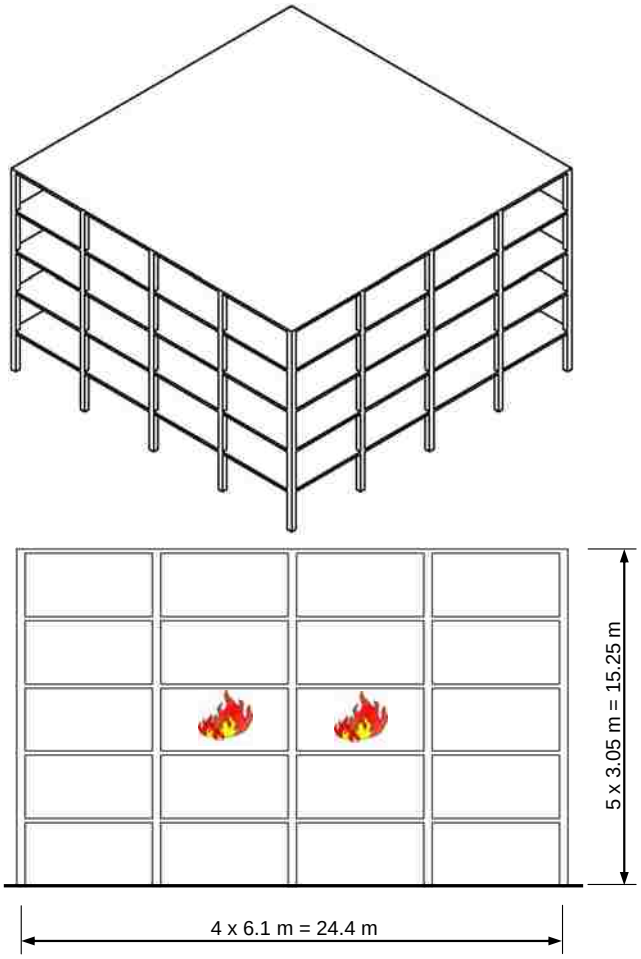

Figure 4-1 Prototype Building

The design layout of slab reinforcement (applied to all stories) is shown in Figure 4-2 for a quarter of the slab based on symmetry. No. 4 bars (diameter = 0.5 in. (12.7 mm)) are used for all slab reinforcement. The slab top reinforcement ratio is 0.53% at the interior slab-column connections and 0.27% at the exterior connections. The design of slab top and bottom reinforcement at the middle strips is governed by the code minimum reinforcement requirements to control cracking due to shrinkage and normal temperature changes. This minimum reinforcement requirement is also enforced for slab top bars because the negative bending moment may be developed over the entire slab at high temperature as shown in Figure 1-6d.

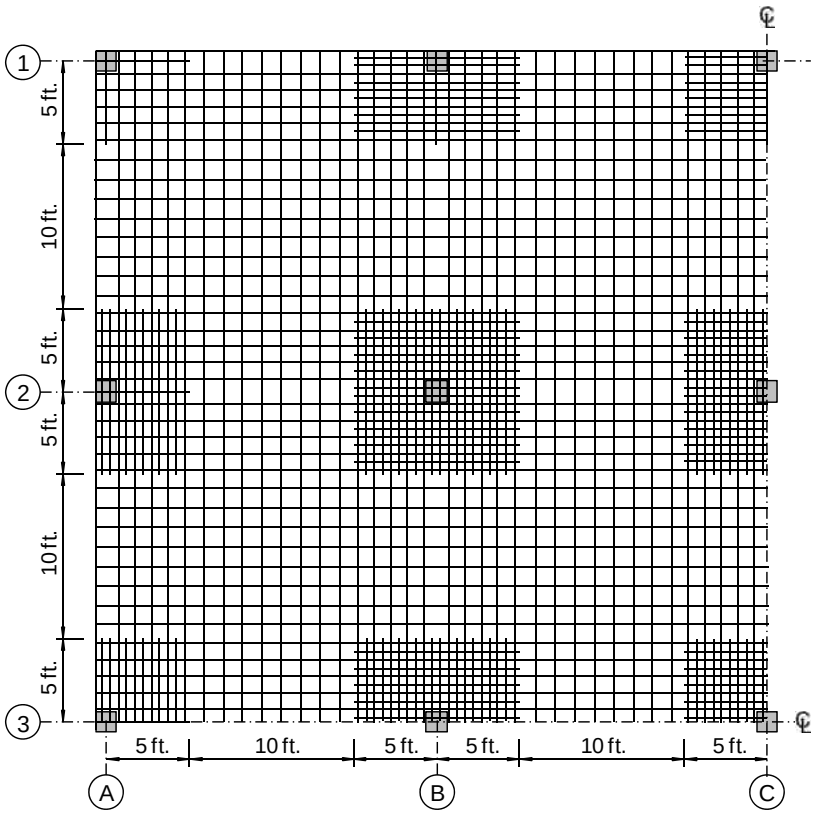

Slab Top Reinforcement

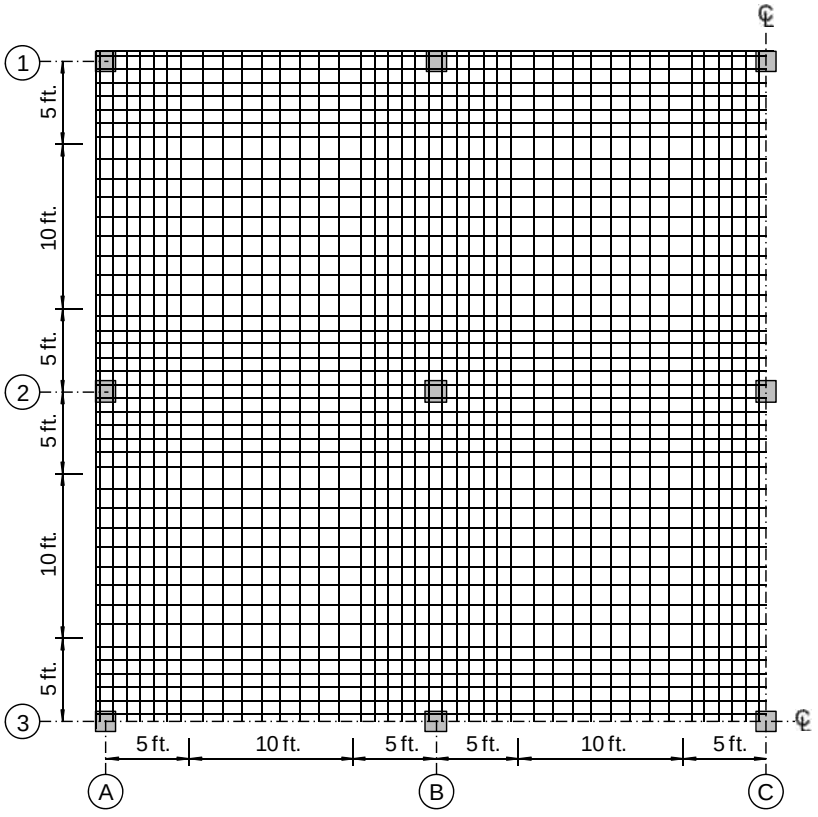

Slab Bottom Reinforcement

Figure 4-2 Slab reinforcement of prototype building

4.2 Finite Element Modeling of Prototype Structure

Finite element analysis is performed using Abaqus (Dassault Systèmes Simulia Corporation, 2009) to estimate the performance of the prototype building in fire conditions. Fire is assumed to occur in the center bays on the third floor. As shown in Figure 4-3, only a quarter of the floor is modeled to reduce computation cost. The prototype slab is unrestrained along the exterior edges and restrained, using five degrees of freedom, along the two slab edges representing the floor centerlines in order to reflect the symmetric property. The columns are fully fixed at the bottom while the top of the columns above the slab are permitted only to move vertically.

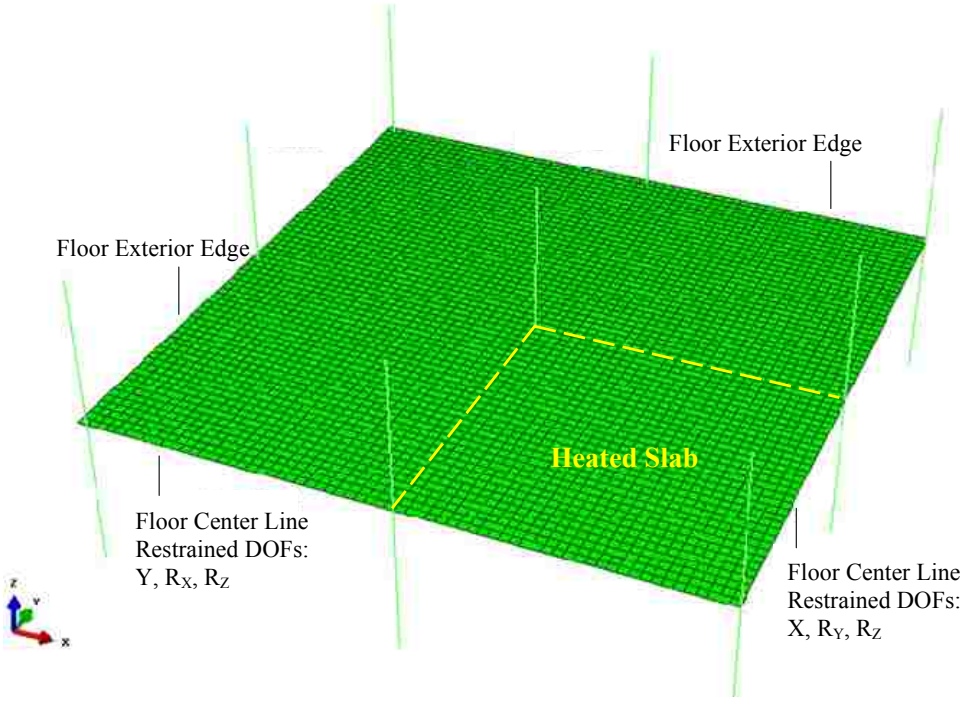

Figure 4-3 Finite element model for prototype building

The thin shell elements and the material properties calibrated in Chapter 3 are used to simulate the reinforced concrete slabs. The mesh size of the shell elements is equal to

slab thickness (medium mesh, Section 3.2.1). Table 4-1 summarizes the definitions of material properties under elevated temperature.

Table 4-1 Summary of Mechanical and Thermal Properties of Slab

	Mechanical Properties						Thermal Properties	
	Density	Poisson's Ratio	Elastic Modulus	Expansion	CDP	Uniaxial Response	Conductivity	Specific Heat
Concrete	2300 kg/m^3	0.2	EC2 (1995) Section 3.1.2.1	Lie (1992) Section 3.2.3	Section 3.1.2.1	EC2 (1995) Section 3.1.2.1	Lie (1992) Section 3.2.2	Lie (1992) Section 3.2.2
Steel	7850 kg/m^3	0.3	EC2 (1995) Section 3.1.2.2	Section 3.1.2.2	N/A	EC2 (1995) Section 3.1.2.2	N/A	N/A

Each column is modeled by five line elements. It is assumed that the fire primarily impacts the slab and no flexural or shear failure occurs in the columns. Therefore, elastic material properties are assigned to these line elements. However, the flexural stiffness of the columns is defined as 70% of that under room temperature to approximately account for (1) concrete cracking in column due to the horizontal expansion of slab, and (2) stiffness reduction of the columns exposed to fire under elevated temperature.

4.3 Results of Heat Transfer Analysis of Prototype Structure

Heat transfer analysis is conducted on the finite element model for the prototype structure. Fire temperatures are assumed identical over the center bays and therefore vary only through the thickness of the slab. The actual temperature in a compartment subjected to fire depends on parameters such as fuel load, radiation, convection, and ventilation. If the standard time-temperature curves such as ISO 834 are directly applied to the slab, it will result in unrealistically conservative prediction of the structural performance of the prototype building. Consequently, the time-temperature history measured at the slab bottom during the furnace testing of Specimen HD12 is applied in the finite element

simulation (Lim & Wade, 2002). Because this study focuses on the behavior of slab, the thermal loading effects on the surrounding columns are not explicitly addressed. However, as mentioned previously, the stiffness of columns is reduced by 30%, which can indirectly consider the stiffness degradation of the columns due to temperature increase.

Figure 4-4 shows the temperature distribution inside the slab determined from heat transfer analysis. The temperature of top reinforcement increases slowly to 129°C at 3 hours. The temperature of bottom reinforcement (located 1 in. (25.4 mm) from slab bottom) increases from the initial 20°C to 657°C at 1.5 hours, and continues to increase to 841°C at 3 hours. According to Figure 2-21, the yield strength of slab bottom reinforcement at 1.5 hours (the design fire resistance for the prototype building) has been reduced to 22% of the yield strength at room temperature. Thus, the elevated temperature at t = 1.5 hours can cause significantly reduced flexural capacity of resisting positive bending moment in the heated slab.

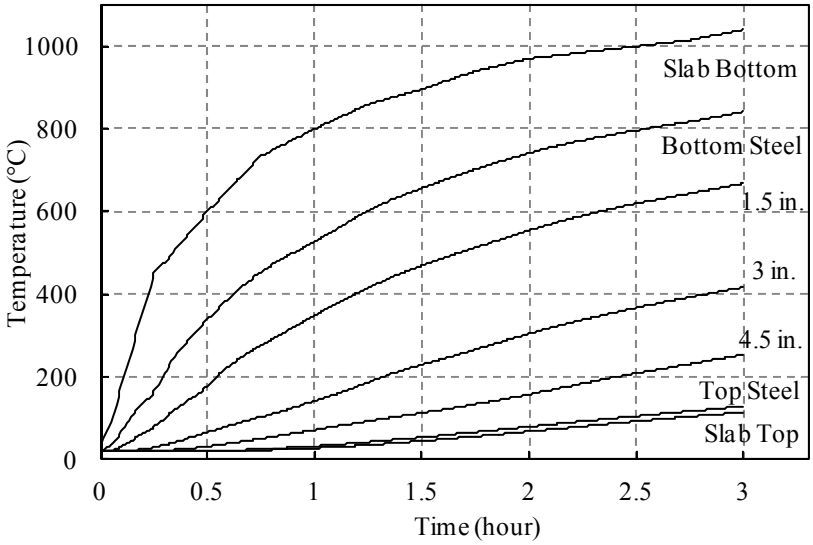

Figure 4-4 Temperature distribution through slab

4.4 Results of Structural Analysis of Prototype Structure

It is assumed that in the event of a fire, the prototype structure is subject to a uniformly distributed gravity load of 1.0D + 0.25L, where D and L are the design dead load and live load described in Section 4.1. Since severe fire is an extreme loading event and some residents of the building may have been evacuated, only 25% of the design live load is considered.

In the analysis, gravity load is applied first and followed by the thermal load determined in the previous section. Due to convergence, the structural analysis of the prototype structure subjected to combined gravity and thermal loading cannot complete the entire 3-hour fire and stops at 95 minutes. However, because the prototype building is designed with 1.5-hour fire resistance, the analysis still provides critical information regarding the fire performance of the structure.

For convenience of presenting analysis results, nine points are identified on the quarter prototype structure shown in Figure 4-5. Points A and I are located at the slab-column interface. Points B and D are located at a distance of 190 mm (7.5 in.) from the column surface. Points H and F are at the center of Columns 3 and 4. Point E is located at the center of the heated slab panel. Points C and G are situated at the mid-span between columns. The slab vertical deflection, in-plane expansion, membrane force, bending moment distribution, rebar force, and rotation near the columns are described in the following sections. Finally, the punching failure potential of slab-column connections is discussed.

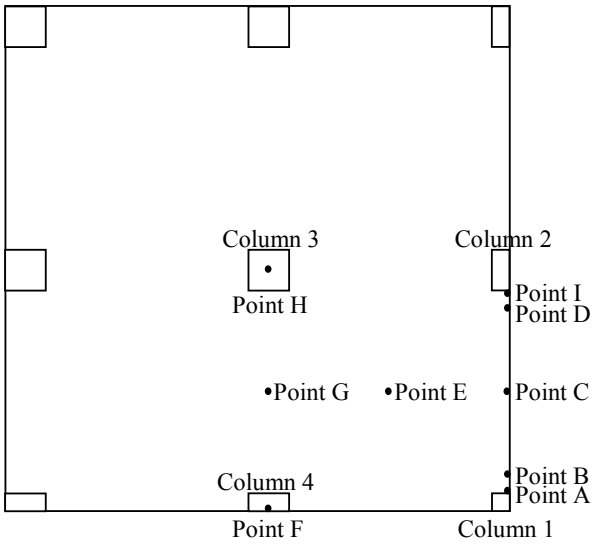

Figure 4-5 Reference diagram for prototype building (showing one quarter of the slab)

4.4.1 Slab Vertical Deflection

Figure 4-6 shows the vertical displacement of the slab at Points C and E. The initial gravity load causes a deflection of 4.79 mm (0.189 in.) and 6.69 mm (0.263 in.) at C and E, respectively. After the thermal load is applied, the deflection at E increases at a higher rate than at C. Upon 95 minutes of heating, the slab deflections at C and E have reached 104 mm (4.09 in.) and 173 mm (6.81 in.), respectively. At this loading stage there is no sign of generating a collapse mechanism associated with flexural yielding because the slab has not experienced a rapid increase in deflection at either location.

The deflected shape of the prototype structure is shown in Figure 4-7 for 0, 30, 60, and 90 minutes of heating. The largest deflection always occurs in the center of the heated slab panel. At t = 90 minutes, the heated slab has formed a 3-D catenary, as if it hangs on the interior columns and column strips. Due to the thermal loading and the resulting load redistribution, the vertical deflection at the adjacent unheated panels is reduced.

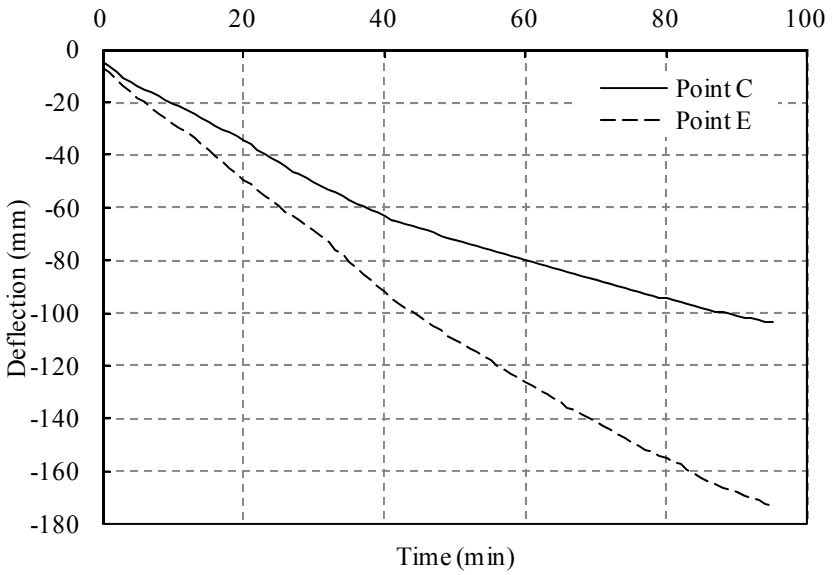

Figure 4-6 Slab vertical deflection at Points C and E

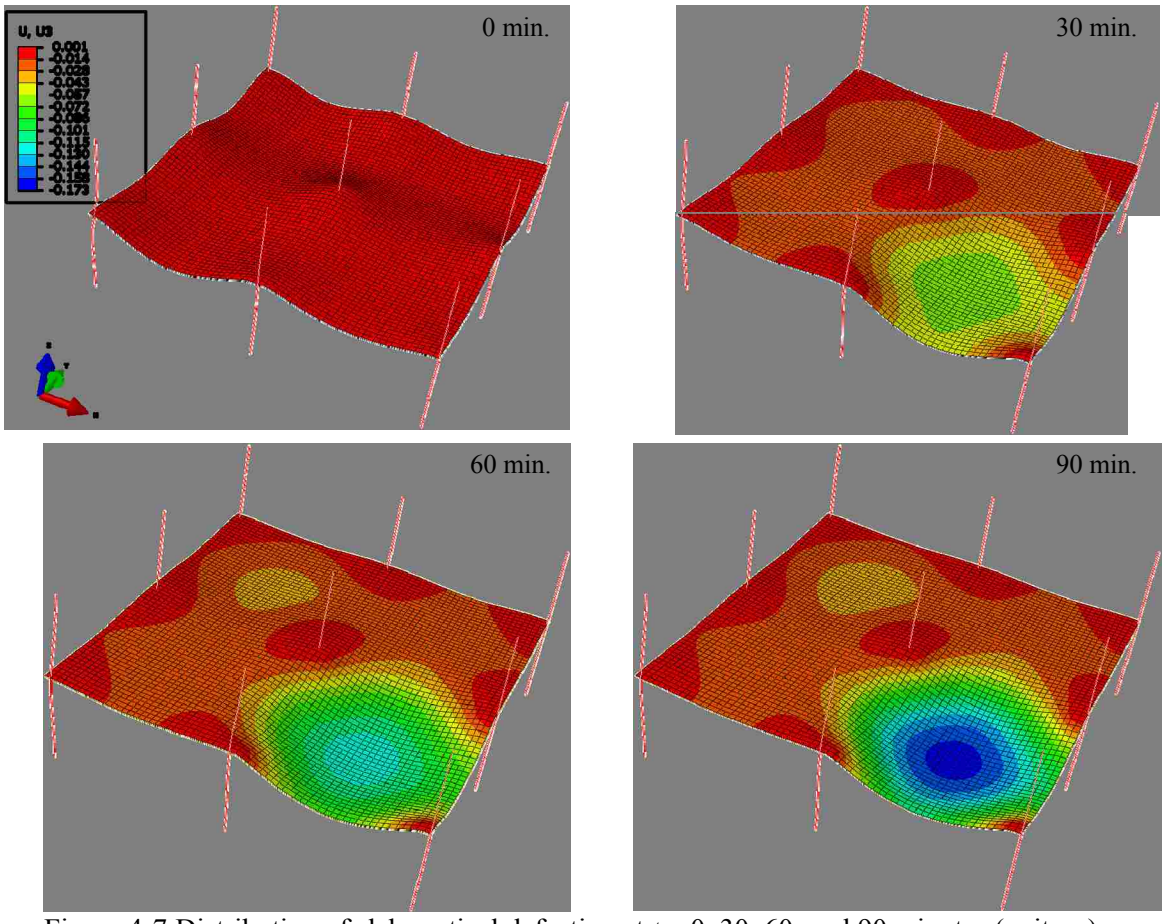

Figure 4-7 Distribution of slab vertical defection at t = 0, 30, 60, and 90 minutes (unit: m)

4.4.2 In-Plane Slab Expansion

Figure 4-8 shows the slab horizontal displacement in the X-direction at Points F, G, and H. The thermal expansion of the heated panel leads to steadily increased outward displacement at all the three locations. Points G and F experience similar in-plane displacements. At t = 90 minutes, the in-plane displacements at F is 21 mm (0.83 in.), a lateral deformation large enough to cause column cracking. Figure 4-9 shows the distribution of horizontal displacement in the entire slab at t = 90 minutes.

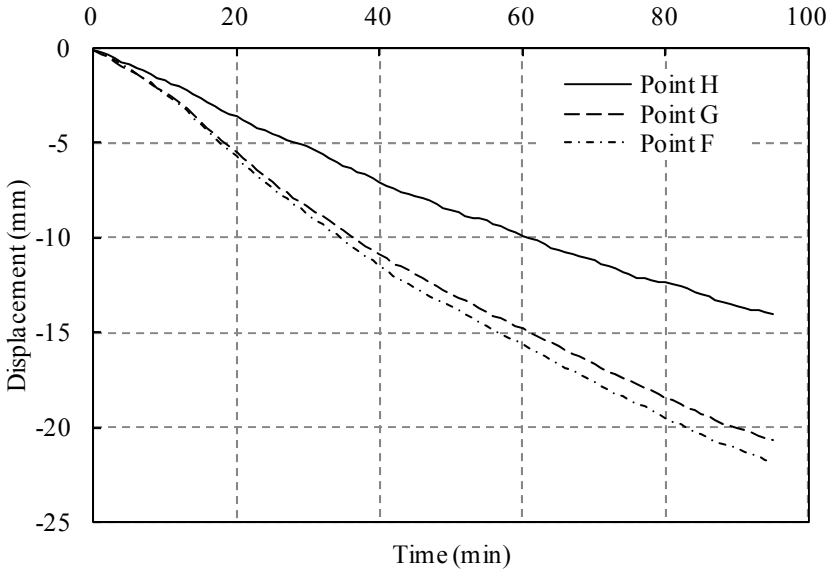

Figure 4-8 Slab horizontal displacement at Points F, G, and H

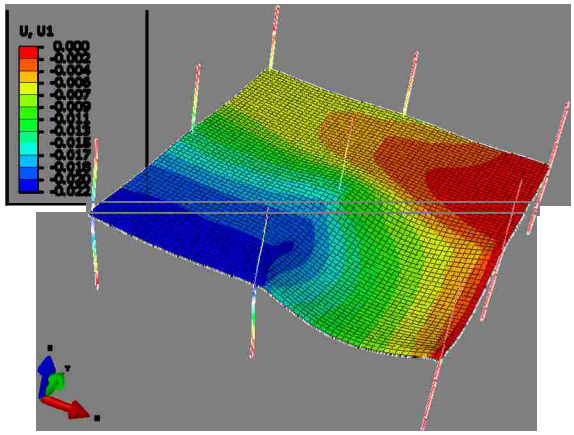

Figure 4-9 Distribution of slab horizontal displacement in X-direction at t = 90 minutes (unit: m)

4.4.3 Membrane Forces in the Slab

Figure 4-10 shows the slab membrane force per unit width in the X-direction at Points A, C and E. Gravity loading causes tensile membrane forces at Points C and E and a compressive membrane force at Point A. However, because the thermal expansion of the heated panel is restrained by the surrounding slab and columns, compressive in-plane forces are developed during thermal loading. After 3 minutes of heating, the slab sections at all three locations are in compression. The rate of increase in compressive force is significantly reduced after 20 minutes of heating for the slab sections at C and E and 30 minutes for slab section A. The largest compressive membrane force always occurs at section A, where the peak compressive membrane force (500 kN/m) is achieved at t = 80 minutes.

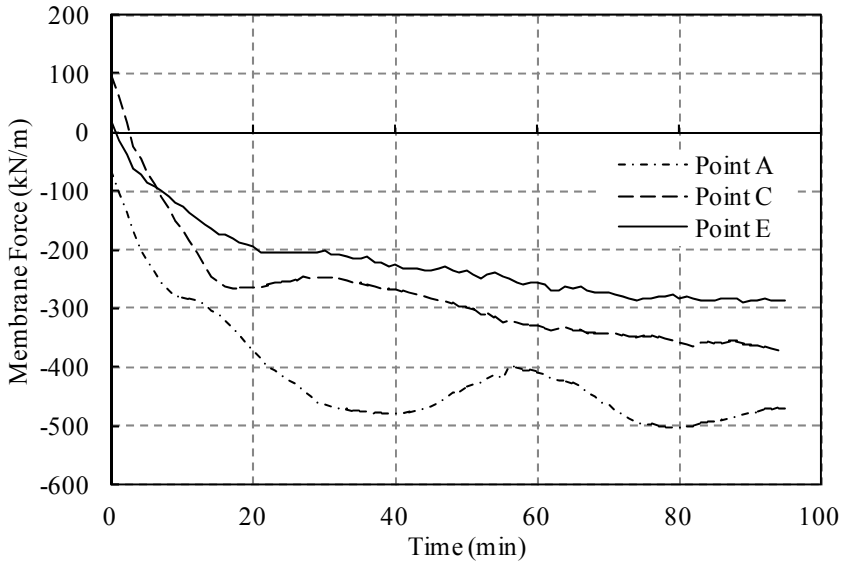

Figure 4-10 Slab membrane forces at Points A, C and E

4.4.4 Bending Moments and Rebar Forces in the Slab

Figure 4-11 shows the bending moments about the X-axis per unit width of slab at Points A, C, E, and I. After gravity load is applied, the slab experiences positive bending

moment (slab bottom in tension, negative sign in Figure 4-11) at mid-span Points C and E, and negative bending moment (slab top in tension, positive sign in Figure 4-11) at column Points A and I. Due to stress concentration, the negative bending moment near columns is much higher than the positive bending moment at C and E.

As the temperature increases, redistribution of bending moment causes the positive moment at Points C and E to switch into negative bending moment. Figure 4-11 indicates that the moment redistribution happens rapidly and causes the slab section near columns (Points A and I) to reach yielding moment at approximately 4 minutes. However, the bending moment of the slab, especially at C and E, change little after 30 minutes of heating. This trend can also be observed in Figure 4-12 for other slab sections located along the line connecting Columns 1 and 2. Figure 4-13 shows the distribution of slab bending moment about X-direction at t = 0, 30, 60, and 90 minutes. It is seen from this figure that moment redistribution also occurs in the unheated slab panels but is much less severe than in the heated slab panel.

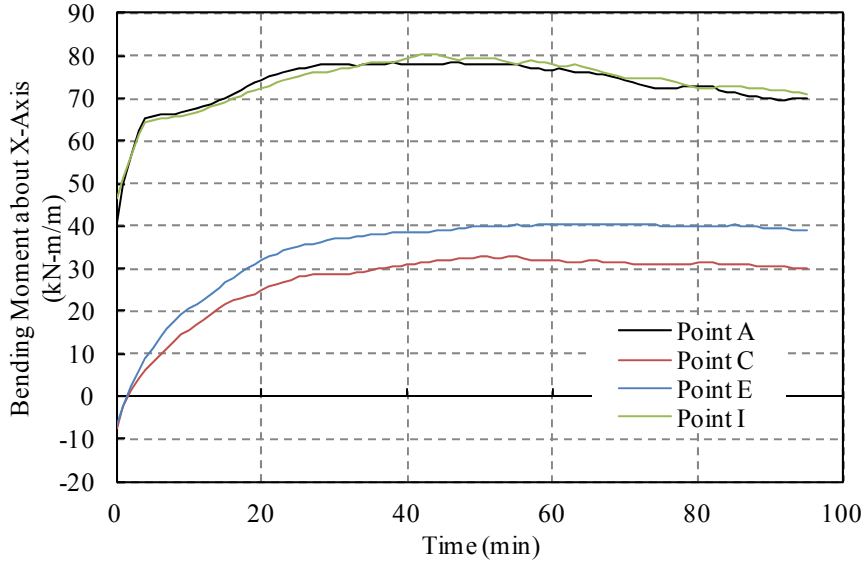

Figure 4-11 Slab bending moment about X-direction at points A, C, E, and I

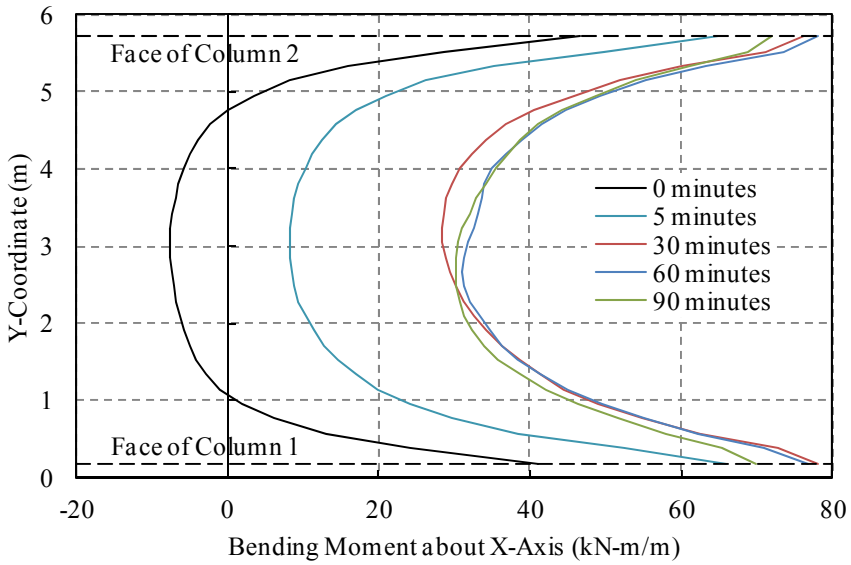

Figure 4-12 Distribution of bending moment about X-axis along line connecting Column 1 and Column 2

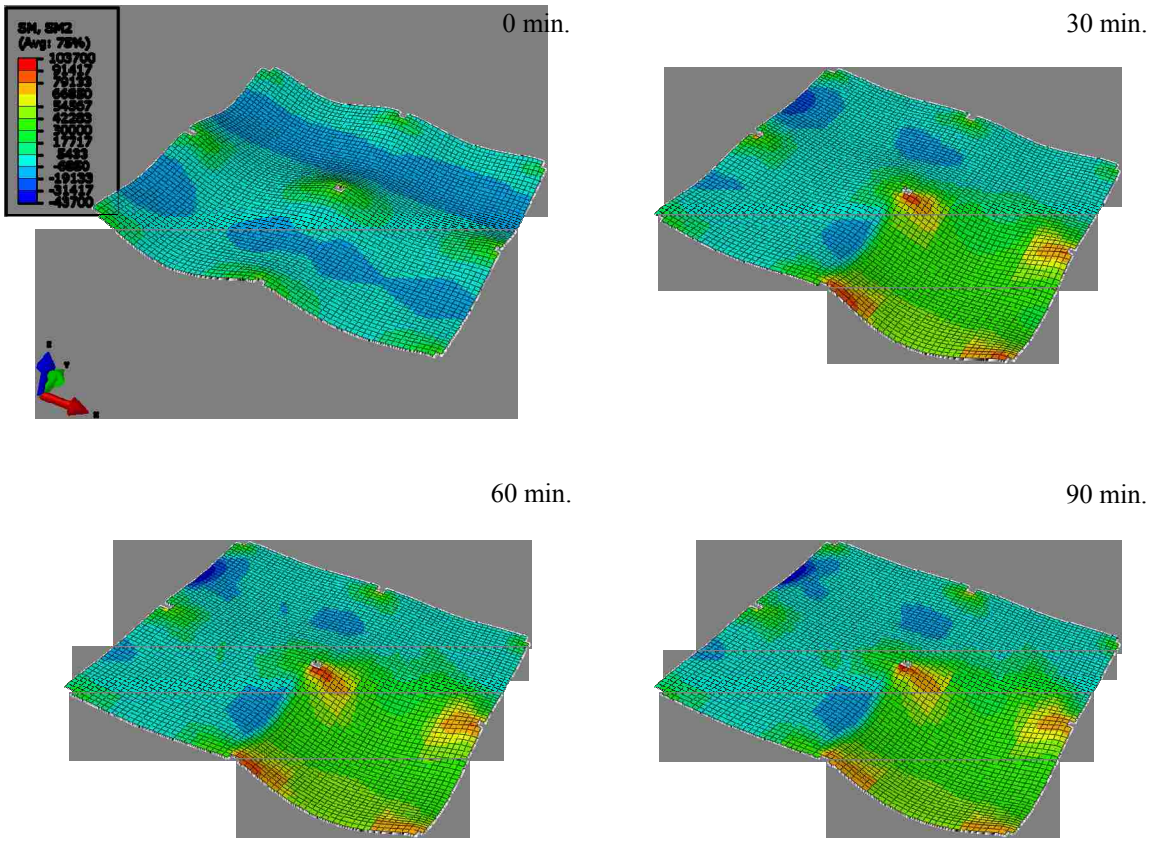

Figure 4-13 Distribution of slab bending moment about X-axis at t = 0, 30, 60, and 90 minutes (unit: N-m/m)

The slab bending moment characteristics can be better understood by examining slab rebar forces. Figure 4-14 shows the force in the slab top and bottom reinforcement resisting moment about the X-axis at Points A, C, E, and I. It is seen that the top reinforcement at slab-column interface (Points A and I) yields at approximately t = 4 minutes, which explains the quick reach of a yield moment as shown in Figure 4-11. The compressive force in bottom bars at these locations keep increasing until t = 40 minutes when the temperature of the bottom bars has exceeded 400˚C and strength degradation of steel has started. Note that the yielding of the slab near the column is caused by restrained slab rotation coupled with thermal gradient, rather than the yielding of bottom reinforcement due to increased temperature. This is because at t = 4 minutes, the temperature of slab bottom reinforcement is less than 100˚C and does not initiate any decrease in yield strength.

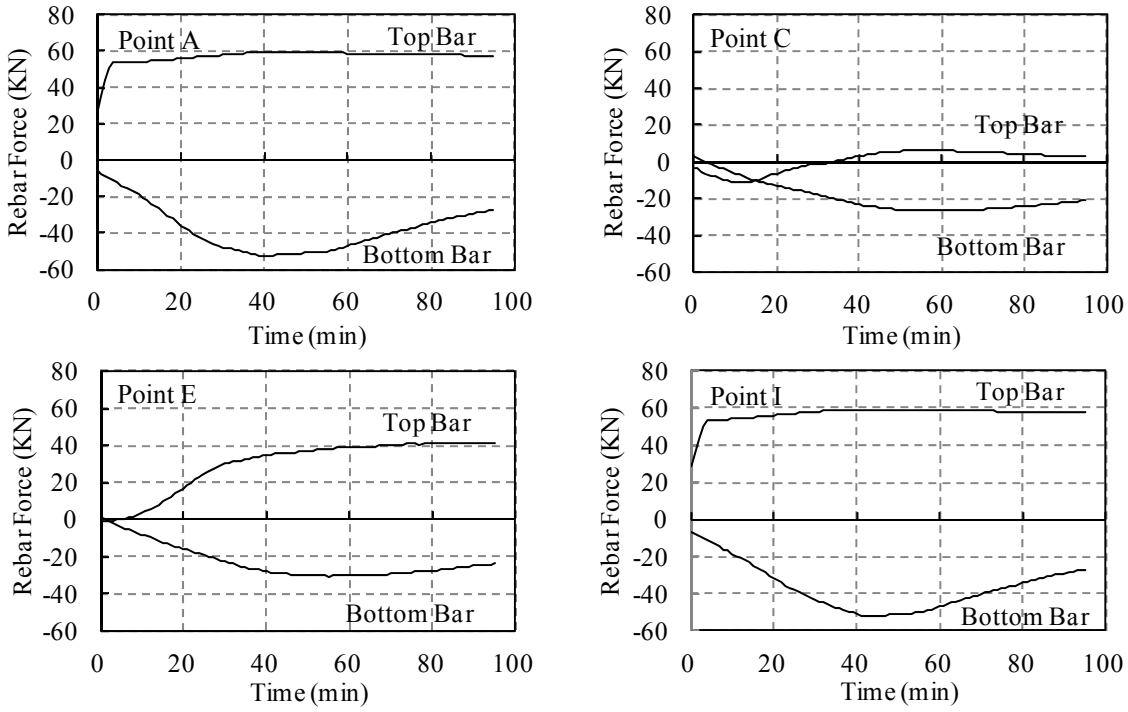

Figure 4-14 Rebar force at Points A, C, E, and I

The quickly developed compressive membrane force at Point C causes increased compressive force in the top reinforcement. However, after 17 minutes, the compressive force decreases and eventually becomes tensile as the positive bending moment is reversed into negative moment. At Point E, located at the center of the heated panel, the initial tensile force in the bottom reinforcement and the compressive force in the top reinforcement quickly change sign. At t = 55 minutes, the compressive force decreases under elevated temperature as its yield strength reduces. However, because all the bottom bars in the heated slab region are in compression, the strength degradation does not cause any distress in terms of the flexural loading capacity of slab.

4.4.5 Slab Section Rotation

The slab section rotates with respect to the X-axis at Points B and D, near the columns as shown in Figure 4-15. This figure indicates that the slab at these locations present a similar response in terms of section rotation. The slab rotation under gravity loading (t = 0) is caused by the flexural deformation of slab near the columns and is negligible. During the initial heating, the slab rotation increases slowly. However, after t = 4 minutes when slab yielding has occurred, slab rotation increases much faster.

Figure 4-16 shows the distribution of slab rotation with respect to the X-axis at t = 30, 60, and 90 minutes. It is seen that slab rotation is highly localized at columns. The deformed shape of the slab and similar rotation contours at the columns surrounding the heated panel clearly indicates that the heated slab in the vicinity of columns deforms as a rigid body.

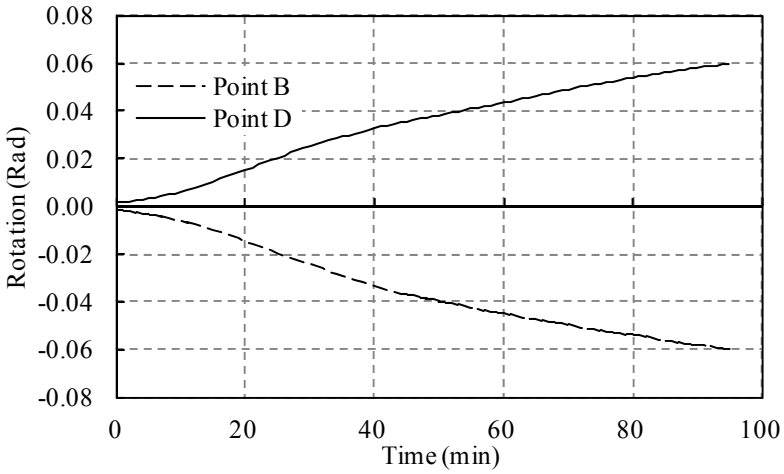

Figure 4-15 Slab rotation at Points B and D

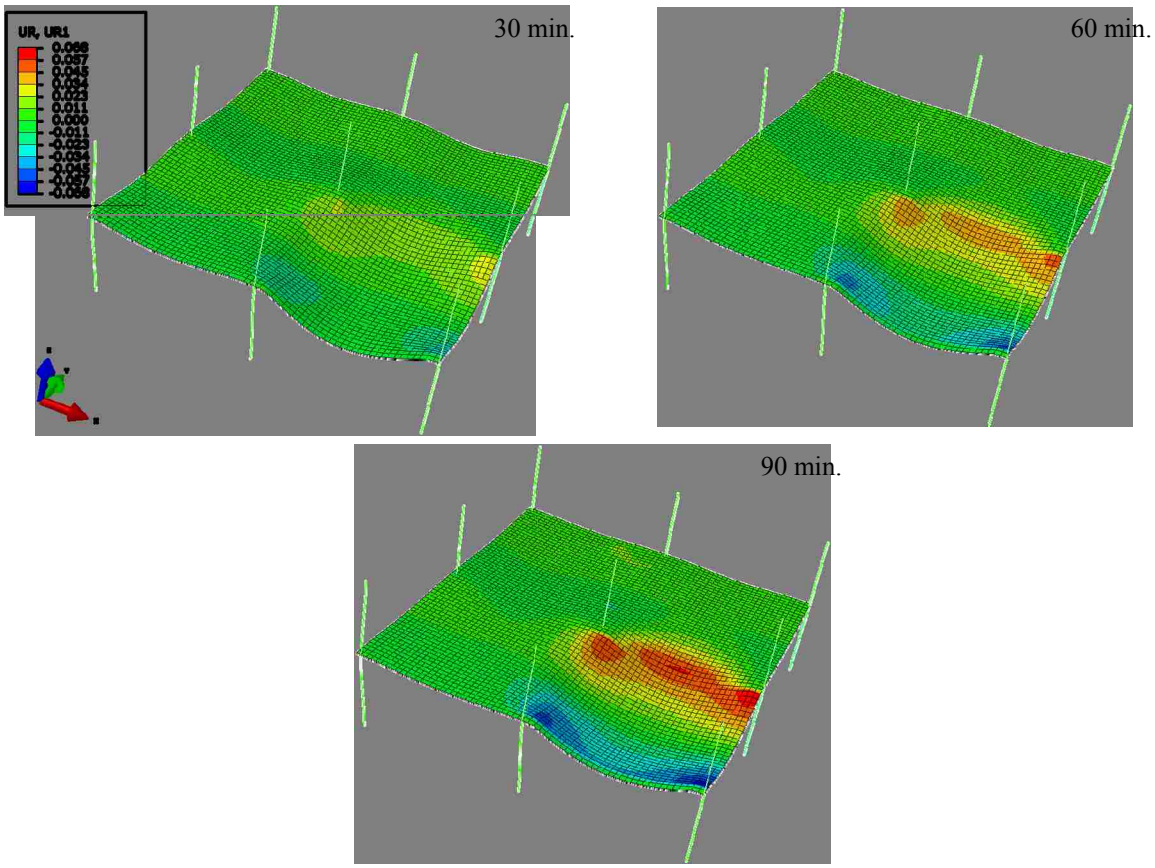

Figure 4-16 Slab rotation distribution (unit: radians)

It shall be noted from Figure 4-15 and Figure 4-16that, at t = 90 minutes, the slab rotation at columns has reached a value as high as almost 0.06 radians. The wide crack opening associated with the large slab rotation probably has deeply extended the inclined crack

and significantly undermined aggregate interlocking force that contributes to connection shear strength. Additionally, none of the isolated slab-column specimens tested previously could survive such a large deformation without any punching failure. Thus, the excessive local deformation of slab poses high risk of punching failure of slab-column connections, as discussed in the following section

4.4.6 Risk of Punching Failure of Slab-Column Connections

There is virtually no test data available for the punching shear strength of flat plate structures under fire conditions. Even for the normal reinforced concrete members such as beams and columns, extremely limited test data exists for shear capacity at high temperatures. EC2 (1995) suggests, when shear reinforcement is provided, the shear strength of a structural member can be determined using the conventional approach with a reduced cross-section, where only the upper portion of the slab is effective to resist shear. However, as shown in Figure 4-17, the inclined shear crack is initiated from slab top surface and the shear resistance can be assumed to be provided mainly by the slab concrete underneath the tip of the inclined crack (the lower portion of slab) (Y. Tian, 2007). Therefore, it is questionable to use the EC2 (1995) approach to estimate the shear strength of slab-column connections under fire.

Figure 4-17 Inclined crack causing punching failure at a slab-column connection (Y. Tian, 2007)

There are other limitations of using the typical code design formulations for punching shear. First, they were developed based on the test data of slab-column connections with supports simulating the inflection points in a flat plate subjected to pure gravity loading. As shown in Figure 1-6d, the inflection points of a slab under fire shift toward the mid-span, leading to an increased shear span that may reduce the load-carrying capacity of the slab-column connection. Further, all the existing formulations for punching resistance have neglected the effects of slab in-plane restraints. However, slab expansion due to concrete cracking and temperature elevation is restrained in an actual flat plate under fire. The slab in-plane restraint may result in greater punching effect as compared to that without in-plane restraining effects.

As indicated in Figure 2-1 and Figure 2-2, a slab prior to punching failure has experienced flexural yielding near the column and behaves as a rigid body. Thus, the punching failure of slab-column connections with low to moderate slab tensile reinforcement ratios can be interpreted as the result of large curvature of the slab near the column. Accordingly, Muttoni's formulation (2008) for the punching strength of slab-column connections without shear reinforcement is adopted in this study. Based on a critical shear crack theory and the data of 99 tests (Figure 4-18), Muttoni (2008) defined the punching strength as a function of the rotation of slab outside the shear crack. According to this theory, the opening of a critical shear crack reduces the capability of concrete under compression to resist punching failure. The width of critical crack was assumed to be proportional to θd, where θ is the rotation of slab and d is effective slab depth. The punching strength V_R was then correlated with slab rotation at failure θ_u as

$$V_R = \left(\frac{3/4}{1 + 15\frac{\theta_u d}{d_{g0} + d_g}} \right) b_0 d\sqrt{f_c} \qquad (\text{in } N, mm \text{ units}) \qquad \text{Equation 4-1}$$

where b_0 is the perimeter of shear critical section taken $d/2$ from the column face, f_c is concrete compressive strength, d_g is the maximum size of the aggregate, and d_{g0} is a reference aggregate size equal to 16 mm.

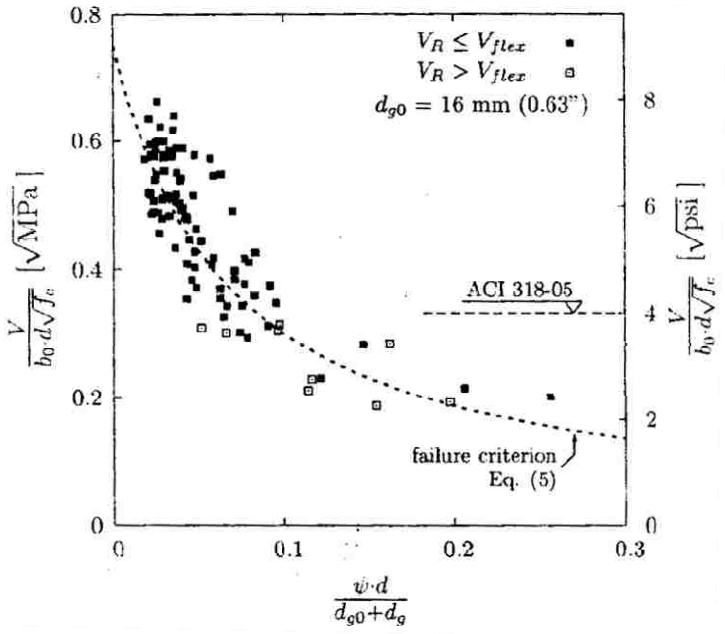

Figure 4-18 Punching shear strength as a function of slab rotation (Muttoni, 2008)

When Equation 4-1 is employed, the concrete strength f_c is defined as a function of temperature. Given that the temperature is not uniformly distributed over slab thickness, the temperature gradient determined from heat transfer analysis (Section 4.34.3) is used to estimate the concrete strength at different locations along the slab depth based on Equations 2-18 and 2-19 given in EC2 (1995). Additionally, it is assumed that the punching strength of a slab-column connection depends primarily on the depth (h_c shown in Figure 4-19) of concrete underneath the inclined crack. Thus, only the slab concrete

within h_c is used to estimate the average concrete strength. Different values of h_c, ranging from 0.1h to 0.9h (where h is slab depth), are assumed because its exact value is difficult to determine.

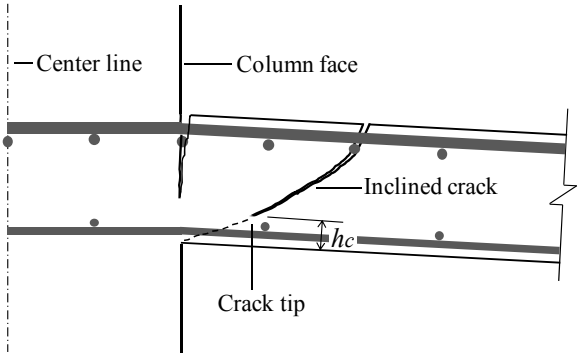

Figure 4-19 Cracking condition of slab-column connection prior to punching failure

Figure 4-20 shows the comparison of shear capacity and shear demand for the center slab-column connection (Column 1) of the prototype structure at t = 30, 60, and 90 minutes of heating. The dashed lines in the figure define the estimated shear capacity V_R with different assumed h_c values. When using Equation 4-1 to calculate V_R, the relative rotation between slab and column at the reference Point A determined from analysis is used to define θ_u. The solid lines in Figure 4-20 give the total shear transferred from slab to the center column and determined from the finite element simulation. Note that this shear demand slightly varies over time due to load redistribution.

It appears from Figure 4-20a that punching shear failure is unlikely to occur within 30 minutes of fire. However, Figure 4-20b indicates that, if the depth of concrete in compression at the incline crack is less than 70% of slab thickness ($h_c < 0.7h$), punching failure may happen within 60 minutes. The specimen shown in Figure 4-17 had a slab tensile reinforcement ratio of 0.5%. It was observed from this test the inclined crack has deeply extended toward the interface of column and slab bottom surface prior to

punching failure (Tian et al., 2008). The prototype structure analyzed in the present study has a similar slab reinforcement ratio (0.53%) at columns. Thus, it is reasonable to assume that $h_c < 0.7h$ and punching failure may occur earlier than 60 minutes of heating. Moreover, as shown in Figure 4-20c, the shear demand at t = 90 minutes is much larger than shear capacity regardless of values assumed for h_c. In summary, the finite element simulation and the use of Equation 4-1 indicate that, although the prototype building is designed with 90 minutes fire resistance, premature punching shear failure may happen due to the large slab local deformation.

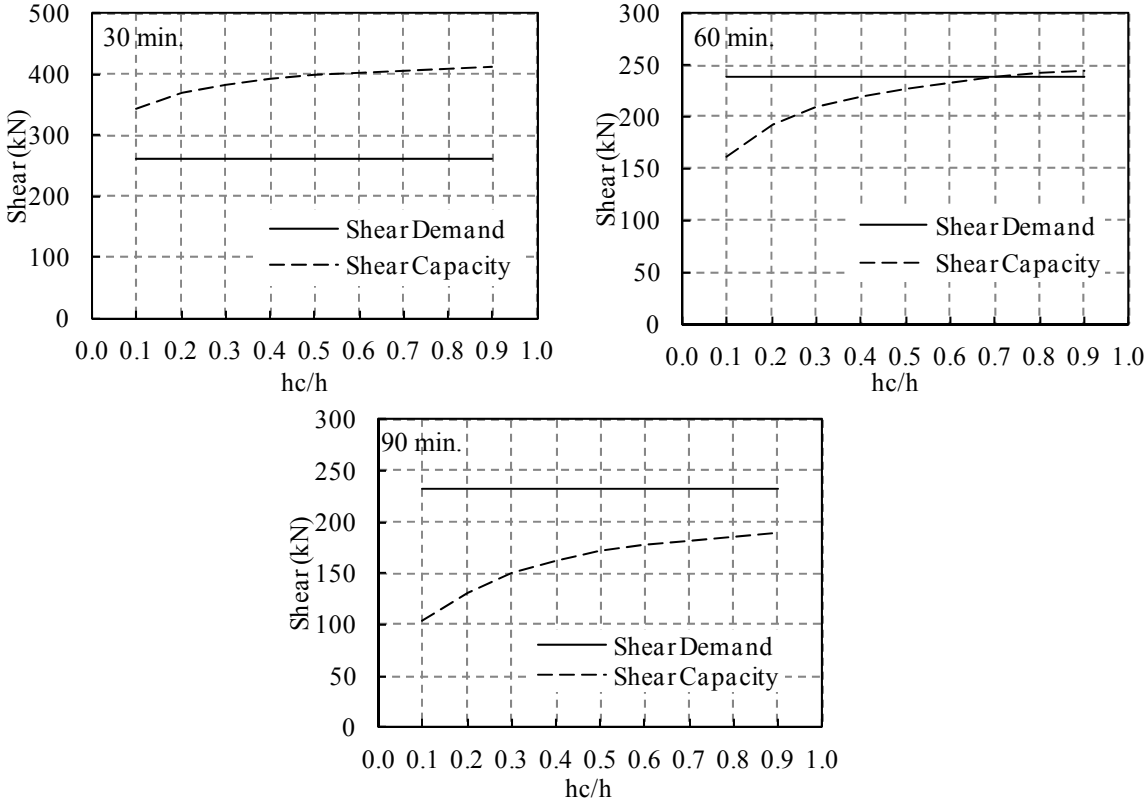

Figure 4-20 Shear capacity *vs*. shear demand at the center slab-column connection at t = 30, 60, and 90 minutes

CHAPTER 5

SUMMARY AND CONLCUSIONS

5.1 RESEARCH SUMMARY

The research presented in this thesis analytically examines the fire performance of flat plate buildings, for which little is known to date. The study contained two phases. First, the modeling parameters for mechanical and thermal properties of materials are calibrated from relevant test data to minimize the uncertainties involved in analysis. Second, the calibrated models are utilized to perform a nonlinear finite element simulation on a flat plate building subjected to fire as well as service level gravity loads. The analysis examines the characteristics of slab deflection, membrane force, bending moment redistribution, and slab rotational deformation near supporting columns. The numerical simulation enables understanding of the structural performance of flat plate under elevated temperature and, more importantly, identifies the likelihood of punching failure at slab-column connections that may trigger large-scale failure in flat plate structures.

5.2 CONCLUSIONS

This study reveals serious concern for the risk of punching failure at the interior slab-column connections of flat plate structures subjected to fire. The analysis carried out on the prototype building indicates that if the depth of concrete underneath the inclined shear crack is less than 70% of the total slab depth, punching failure may have occurred at 60 minutes of heating. This is because the shear demand at the interior connection has exceeded the shear capacity. After 90 minutes of fire loading, the shear demand will be much higher than the shear capacity, even when 90% of the slab section is assumed as

effective to resist shear. Therefore, it is reasonable to conclude that prior to the reach of design fire resistance, a premature punching shear failure may have occurred due to the large curvature of the slab near the column.

The analysis also indicates that the slab top reinforcement near the columns yields quickly, around 4 minutes of heating, due to the restraint of thermal-induced slab rotational deformation by columns. As a result of rapid yielding of reinforcement at columns, the heated slab experiences severe bending moment redistribution which changes positive bending moment, caused initially by gravity loading, at the mid-span into negative moment. However, very little change in bending moment is seen between 30 to 90 minutes of heating. Due to the restrained thermal expansion, membrane forces in the slab become compressive at all sections after only a short period of thermal loading. Moreover, no collapse mechanism associated with slab flexural yielding is produced at 90 minutes of thermal loading.

5.3 Recommendations for Future Work

This study is limited to flat plates where the design is governed by gravity loads and the slabs are supported on square columns without using any shear reinforcement. Additionally, severe convergence problems were encountered in the analysis. It is recommended that future work of flat plate structures under fire loading address the following issues:

(1) Experiment data on the punching shear strength of slab-column connections (with and without shear reinforcement) under elevated temperature. Such data does not exist and is urgently needed to assess the fire safety of flat plate structures.

(2) The behavior of flat plate structures with varied time-temperature histories and gravity load levels.

(3) The fire performance of flat plate structures with different slab reinforcement layouts such as discontinuous slab top reinforcement.

(4) More robust material models for concrete and steel under elevated temperature to achieve better convergence of numerical simulations.

REFERENCES

ACI Committee 318, American Concrete Institute, & International Organization for Standardization. (2008). *Building code requirements for structural concrete (ACI 318-08) and commentary*. Farmington Hills, Mich.: American Concrete Institute.

American Society of Civil Engineers, & ebrary, I. (2010). *Minimum design loads for buildings and other structures*. Reston, VA: American Society of Civil Engineers. Retrieved from http://www.library.unlv.edu/help/remote.html;

Anderberg, Y., & Thelandersson, S. (1976). Stress and deformation characteristics of concrete, 2- experimental investigation and material behaviour model.*Bulletin 54*, 9/1/2011.

Bietel, J., & Iwankiw, N. (2008). *Analysis of needs and existing capabilities for full-scale fire resistance testing.* (). Gaithersburg, MD: National Institute of Standards and Technology (NIST). Retrieved from http://www.fire.nist.gov/bfrlpubs/fire02/art028.html

Buchanan, A. H. (2001). *Structural design for fire safety*. Chichester West Sussex, England; New York: J. Wiley.

CRSI Committee of Fire Ratings. (1980). In Gustafson D. P. (Ed.), *Reinforced concrete fire resistance* Concrete Reinforcing Steel Institute.

Dassault Systèmes Simulia Corporation. (2009). *Abaqus 6.9 documentation*

Elstner, R. C., & Hognestad, E. (1956). Shearing strength of reinforced concrete slabs. *ACI Journal, 53*(1), 29-58.

European Committee for Standardization. (1995a). *Eurocode 2: Design of concrete structures. ENV 1992: Part 1-2: General rules-structural fire design.* Retrieved 05/20, 2011, from http://www.scribd.com/doc/31503917/Eurocode-2-1-2-1996-EN

European Committee for Standardization. (1995b). *Eurocode 3: Design of steel structures. ENV 1993: Part 1-2: General rules-structural fire design.* Retrieved 09/01, 2011, from http://www.scribd.com/doc/29029236/Eurocode-3-1-2

European Committee for Standardization. (1996). *Eurocode 1: Basis of design and action on structures. ENV 1991: Part 2-2: Actions on structures exposed to fire.* Retrieved 08/20, 2011, from http://www.scribd.com/doc/59072215/Eurocode-1-2-2

Factory fire kills 15 in egypt. (2000). Retrieved August, 4, 2011, from http://news.bbc.co.uk/2/hi/asia-pacific/843604.stm

Fletcher, I. A., Welch, S., Torero, J. L., & Usmani, A. (2007). Behavior of concrete structures in fire. *Thermal Science, 11*(2), 37-52.

Gardner, N. J., & Shao, X. -. (1996). Punching shear of continuous flat reinforced concrete slabs. *ACI Structural Journal, 93*(2), 218-228.

Ghaffar, A., Chaudhry, M. A., & Ali, M. K. (2005). A new approach for measurement of tensile strength of concrete. *Journal of Research (Science), 16*(1), 01-09. Retrieved from http://www.bzu.edu.pk/jrscience/vol16no1/1.pdf

Guandalini, S., Burdet, O. L., & Muttoni, A. (2009). Punching tests of slabs with low reinforcement ratios. *ACI Structural Journal, 106*(1), 87-95.

Harmathy, T. Z. (1993). *Fire safety design and concrete*. Harlow, Essex, England: Longman Scientific & Technical.

Hognestad, E. (1953). Yield-line theory or ultimate flexural strength of reinforced concrete slabs. *American Concrete Institute -- Journal, 24*(7), 637-656.

Joint ACI/TMS Committee 216, American Concrete Institute, & International Organization for Standardization. (2007). *Code requirements for determining fire resistance for concrete and masonry construction assemblies*. Farmington Hills, Mich.: American Concrete Institute.

Kirby, B. R., & Preston, R. R. (1988). High temperature properties of hot-rolled, structural steels for use in fire engineering design studies. *Fire Safety Journal, 13*(1), 27-37. doi:DOI: 10.1016/0379-7112(88)90030-6

Lie, T. T. (Ed.). (1992). *Structural fire protection* (Technical Report No. 78 ed.). New York: American Society of Civil Engineers.

Lim, L., & Wade, C. (2002). *Experimental fire tests of two-way concrete slabs.* (). University of Canterbury:

Lim, L., Buchanan, A., Moss, P., & Franssen, J. -. (2004). Numerical modelling of two-way reinforced concrete slabs in fire. *Engineering Structures, 26*(8), 1081-1091. doi:10.1016/j.engstruct.2004.03.009

Lubliner, J., Oliver, J., Oller, S., & Oñate, E. (1989). A plastic-damage model for concrete. *International Journal of Solids and Structures, 25*(3), 299-326.

Meacham, B., Engelhardt, M., & Kodur, V. (2009). *Collection of data on fire and collapse, faculty of architecture building, delft university of technology* Retrieved from http://www.europeanfireacademy.com/cms/show/id=710654

Moss, P. J., Dhakal, R. P., Wang, G., & Buchanan, A. H. (2008). The fire behaviour of multi-bay, two-way reinforced concrete slabs. *Engineering Structures, 30*(12), 3566-3573. doi:10.1016/j.engstruct.2008.05.028

Muttoni, A. (2008). Punching shear strength of reinforced concrete slabs without transverse reinforcement. *ACI Structural Journal, 105*(4), 440-450.

National Institute of Standards and Technology, & United States. (2005). *Final report on the collapse of the world trade center towers*. Gaithersburg, Md.: U.S. Dept. of Commerce, Technology Administration, National Institute of Standards and Technology.

Nilson, A. H., Darwin, D., & Dolan, C. W. (2003). *Design of concrete structures* (13th ed.). New York: McGraw-Hill.

Papaioannou, K. (1986). The conflagration of two large department stores in the centre of athens. *Fire and Materials, 10*(3-4), 4 August 2011-177. Retrieved from http://onlinelibrary.wiley.com.ezproxy.library.unlv.edu/doi/10.1002/fam.810100312/pdf

Park, R., & Gamble, W. L. (2000). *Reinforced concrete slabs* (2nd ed.). New York: Wiley.

Purkiss, J. A. (1996). *Fire safety engineering design of structures*. Oxford England; Boston: Butterworth-Heinemann.

Russian apartment block collapses. (2002). Retrieved June 3, 2010, from http://news.bbc.co.uk/2/hi/europe/2023544.stm

Schneider, U. (1988). Concrete at high temperatures — A general review. *Fire Safety Journal, 13*(1), 55-68. doi:DOI: 10.1016/0379-7112(88)90033-1

Shehata, I. A. E. M. (1990). Simplified model for estimating the punching resistance of reinforced concrete slabs. *Materials and Structures, 23*(5), 364-371. doi:10.1007/BF02472716

Shehata, I. A. E. M., & Regan, P. E. (1989). Punching in R.C. slabs. *Journal of Structural Engineering New York, N.Y., 115*(7), 1726-1740.

Sherif, A. G., & Dilger, W. H. (1996). Critical review of the CSA A23.3-94 punching shear strength provisions for interior columns. *Canadian Journal of Civil Engineering, 23*(5), 998-1011.

Tian, Y. (2007). *Behavior and modeling of reinforced concrete slab-column connections.* (Unpublished Doctoral dissertation). University of Texas at Austin, Austin, TX.

Tian, Y., Jirsa, J. O., Bayrak, O., Widianto, & Argudo, J. F. (2008). Behavior of slab-column connections of existing flat-plate structures. *ACI Structural Journal, 105*(5), 561-569.

Vermeer, P. A., & De Borst, R. (1984). Non-associated plasticity for soils, concrete, and rock. *HERON, 29*

Wang, B., Dong, Y., & Gao, L. (2011). *Fire experimental study of four-edge fixed reinforced concrete slab in fire* (Guangzhou ed.) doi:10.4028/www.scientific.net/AMR.163-167.1626

Wang, G. (2006). *Performance of reinforced concrete flat slabs exposed to fire.* (Unpublished Master of Engineering in Fire Engineering). University of Canterbury, Christchurch, New Zealand.

VITA

Graduate College
University of Nevada, Las Vegas

Sara Jean George

Degrees:

Bachelor of Science in Architectural Engineering, Structural Emphasis 2007
University of Wyoming

Employment:

Summer Intern ARUP	Summer 2010 Houston, Texas
Project Engineer Barker Drottar Associates	May 2007- June 2009 Las Vegas, Nevada
Summer Intern Structural Engineers, P.C.	Summer 2006 Marshalltown, Iowa

Thesis Title:
Structural Performance of Reinforced Concrete Flat Plate Buildings Subjected to Fire

Thesis Examination Committee:
Chairperson, Dr. Ying Tian, Ph.D., P.E.
Committee Member, Dr Samaan Ladkany, Ph.D., P.E.
Committee Member, Dr Aly Said, Ph.D., P.E.
Graduate Faculty Representative, Dr. Brendan O'Toole, Ph.D.